bioRxiv preprint doi: https://doi.org/10.1101/2020.06.05.135905; this version posted June 6, 2020. The copyright holder for this preprint (which was not certified by peer review) is the author/funder. All rights reserved. No reuse allowed without permission.

Anesthetics uniquely decorrelate hippocampal network activity, alter spine dynamics and affect memory consolidation

Wei Yang[1,6], Mattia Chini[2,6], Jastyn A. Pöpplau[2], Andrey Formozov[1], Patrick Piechocinski[1], Cynthia Rais[1], Fabio Morellini[3], Olaf Sporns[4,5], Ileana L. Hanganu-Opatz[2] and J. Simon Wiegert[1*]

[1]Research Group Synaptic Wiring and Information Processing, Center for Molecular Neurobiology Hamburg, University Medical Center Hamburg-Eppendorf, 20251 Hamburg, Germany

[2]Developmental Neurophysiology, Center for Molecular Neurobiology, University Medical Center Hamburg-Eppendorf, 20251 Hamburg, Germany

[3]Research Group Behavioral Biology, Center for Molecular Neurobiology Hamburg, University Medical Center Hamburg-Eppendorf, 20251 Hamburg, Germany

[4]Department of Psychological and Brain Sciences, Indiana University, Bloomington, Indiana, USA

[5]Indiana University Network Science Institute, Indiana University, Bloomington, Indiana, USA

[6]These authors contributed equally

*Correspondence: simon.wiegert@zmnh.uni-hamburg.de, @SimWieg

SUMMARY

General anesthesia is characterized by reversible loss of consciousness accompanied by transient amnesia. Yet, long-term memory impairment is an undesirable side-effect. How different types of general anesthetics (GAs) affect the hippocampus, a brain region central to memory formation and consolidation, is poorly understood. Using extracellular recordings, chronic 2-photon imaging and behavioral analysis, we monitor the effects of isoflurane (Iso), medetomidine/midazolam/fentanyl (MMF), and ketamine/xylazine (Keta/Xyl) on network activity and structural spine dynamics in the hippocampal CA1 area of adult mice. GAs robustly reduced spiking activity, decorrelated cellular ensembles, albeit with distinct activity signatures, and altered spine dynamics. Iso anesthesia most closely resembled wakefulness, and network alterations recovered more readily than with Keta/Xyl and MMF. Correspondingly, memory consolidation was impaired after exposure to Keta/Xyl and MMF, but not Iso. Thus, different anesthetics distinctly alter hippocampal network dynamics, synaptic connectivity, and memory consolidation, with implications for GA strategy appraisal in animal research and clinical settings.

KEYWORDS

General anesthesia, isoflurane, ketamine, fentanyl, hippocampus, population dynamics, network activity, spine turnover, episodic memory

bioRxiv preprint doi: https://doi.org/10.1101/2020.06.05.135905; this version posted June 6, 2020. The copyright holder for this preprint (which was not certified by peer review) is the author/funder. All rights reserved. No reuse allowed without permission.

INTRODUCTION

General anesthesia is a drug-induced, reversible behavioral condition encompassing unconsciousness, amnesia, sedation, immobility, and analgesia (Rudolph and Antkowiak, 2004; Urban and Bleckwenn, 2002). Together, these aspects represent a state where surgery can be tolerated without the requirement for further drugs (Urban and Bleckwenn, 2002). The behavioral effects of GAs are dose-dependent. At clinical (i.e. highest) dosage, they should induce unconsciousness, even though experimental evidence of this phenomenon is challenging to collect (in absence of a verifiable consciousness theory). At lower doses, some GAs cause unresponsiveness and loss of working memory, phenomena that have been both hypothesized to potentially confound the apparent loss of consciousness (Alkire et al., 2008; Sanders et al., 2012). At much lower doses still, GAs cause profound retrograde amnesia. When general anesthesia fails to induce such behavioral effects, intraoperative awareness ensues, a condition that is associated with long-term negative health consequences (Mashour et al., 2011). While loss of memory is required for the time period of anesthesia, so that no memories of the surgical procedure are formed (Antognini and Carstens, 2002; Rudolph and Antkowiak, 2004), long-term impairments of retrograde or anterograde memories are not desired. Although general anesthesia is generally considered a safe procedure, growing literature points to the possibility of long-term negative effects on the central nervous system (Vutskits and Xie, 2016). This is particularly true for specific categories of patients, such as the elderly, infants and children (Vutskits and Xie, 2016). Among the observed side effects, the most common are post-operative cognitive dysfunction syndromes, including post-operative delirium (POD) and post-operative cognitive decline (POCD). Post-operative cognitive disturbances are positively correlated with the duration of anesthesia and a single exposure to GAs can cause retrograde and anterograde memory deficits that persist for days to weeks in rodent models (Zurek et al., 2014). These aspects point to a generalized action of GAs on the memory system.

Given that amnesia is a fundamental part of general anesthesia and that the hippocampus controls memory formation and consolidation, it is important to understand how anesthetics affect hippocampal function. Together with subiculum, the CA1 area constitutes the main hippocampal output region. CA1 pyramidal cells receive excitatory input mainly from CA3 (in strata oriens & radiatum) and layer 3 of entorhinal cortex at spine synapses (Neves et al., 2008), relaying information about external and internal state, respectively (Larkum, 2012). Thus, CA1 pyramidal cells have been suggested to integrate information about the environment and internal representations (Bittner et al., 2015; Larkum, 2012), with synaptic spines being possible sites of memory storage (Frey and Morris, 1997; Kasai et al., 2010; Segal, 2005; Yang et al., 2009). Moreover, dynamic modulation of spine stability has been linked to synaptic plasticity (De Roo et al., 2008; Nagerl et al., 2004; Wiegert and Oertner, 2013; Wiegert et al., 2018). Synaptic plasticity, in turn, underlies learning and memory formation (Whitlock et al., 2006), suggesting that spine turnover in the hippocampus directly reflects these processes (Attardo et al., 2015; Schmid et al., 2016). Considering the low concentrations of anesthetics required to induce amnesia, these compounds are thought of affecting in particular the hippocampus. One possible explanation of this sensitivity is the fact that a class of γ-aminobutyric acid receptors (GABARs), which is strongly modulated by some anesthetics, is predominantly expressed in the hippocampus (Bonin and Orser, 2008; Sur et al., 1999). However, a systematic, in-depth investigation of the effects of anesthetics on the hippocampus bridging synaptic, network and behavioral levels, is still lacking.

bioRxiv preprint doi: https://doi.org/10.1101/2020.06.05.135905; this version posted June 6, 2020. The copyright holder for this preprint (which was not certified by peer review) is the author/funder. All rights reserved. No reuse allowed without permission.

Here, using behavioral analysis, extracellular recordings and chronic 2-photon calcium imaging, we systematically assessed how memory performance, CA1 network dynamics and synaptic structure are affected by three commonly used combinations of GAs: isoflurane (Iso), midazolam/medetomidine/fentanyl (MMF), and ketamine in combination with xylazine (Keta/Xyl). All three GAs strongly reduced overall neuronal spiking and, opposite to what has been found in the neocortex (Goltstein et al., 2015; Greenberg et al., 2008; Wenzel et al., 2019), decorrelated network activity, leading to a fragmented network state. However, the induced patterns of activity were highly distinct between the three different conditions and recovered to the pre-anesthetic status with disparate rates. Testing the effect of repeated anesthesia on spine dynamics revealed that Keta/Xyl, the condition which most strongly affected calcium activity, significantly reduced spine turnover, leading to an overall (over)stabilization of hippocampal synapses. In contrast, Iso and MMF mildly increased spine turnover. Finally, we show that the two anesthetic conditions which induce longer-lasting network alterations, Keta/Xyl and MMF, negatively influenced hippocampus-dependent memory consolidation. Thus, different anesthetics, despite reaching a similar physiological state, strongly differ in their effects on synaptic stability, hippocampal network activity, and memory consolidation.

RESULTS

Iso, Keta/Xyl and MMF induce distinct patterns of network activity

Iso, Keta/Xyl and MMF have distinct molecular targets and modes of action in the brain. We therefore hypothesized that electrical activity in the hippocampus is uniquely altered by each of the three anesthesia strategies. To test this hypothesis, we investigated local field potentials (LFPs) and firing of individual neurons (single unit activity, SUA) extracellularly recorded in the CA1 area of dorsal hippocampus (dCA1) during wakefulness followed by 45 min of anesthesia and 45 min of recovery (Fig. 1A, S1A). We found that the anesthetics differently affected network activity, inducing characteristic modulation of various frequency bands (Fig. 1B). During wakefulness, LFP power in CA1 was highest in the theta (4-12 Hz) and low-gamma (40-60 Hz) bands (Fig. S1B). Exposure to 2-2.5% Iso led to a strong reduction of LFP power > 4 Hz within the first 2 minutes that was accompanied by complete loss of mobility of the animal (Fig. 1C, S1B,C). Similarly, MMF injection promptly decreased LFP power in the same frequency bands. In contrast, Keta/Xyl increased power across all frequencies during the first 10 min after injection, the most prominent effect being observed for activity at 5-30 Hz. This is consistent with previous reports, finding enhanced theta and low-gamma power in CA1 of rats under ketamine anesthesia (Soltesz and Deschenes, 1993). The initial LFP power increase was followed by a gradual, significant decrease of 30-100 Hz activity (Fig. 1C, S1B,C).

It is widely accepted that, in the neocortex, GAs favor slow oscillations at the expense of faster ones (Purdon et al., 2015). To determine whether this is also the case in the hippocampus, we next asked how the investigated anesthetics affect slow network oscillations. Consistent with previous reports (Collins et al., 2001; Contreras and Steriade, 1995; Steriade et al., 1993), Keta/Xyl strongly enhanced LFP power at 0.5-4 Hz throughout the entire recording period (Fig. 1C,D, S1C), but suppressed frequencies lower than 0.5 Hz. In contrast, Iso strongly augmented LFP power below 0.5 Hz, peaking at 0.1-0.2 Hz (Fig. 1C,D, S1C), whereas MMF induced no significant increase in the low-frequency regime. However, similar to Keta/Xyl, a significant reduction was present below 0.5 Hz, which persisted throughout the entire recording period (Fig. 1C,D). The power-law decay exponent (1/f slope) of the LFP power spectrum has

bioRxiv preprint doi: https://doi.org/10.1101/2020.06.05.135905; this version posted June 6, 2020. The copyright holder for this preprint (which was not certified by peer review) is the author/funder. All rights reserved. No reuse allowed without permission.

been hypothesized to track excitation/inhibition (E/I) balance, and is reduced under anesthesia (Gao et al., 2017), indicating a shift towards inhibition. Considering the robust effects on LFP power that we reported, we reasoned that a similar phenomenon might also occur in the hippocampus. Indeed, all anesthetics significantly decreased the power-law decay exponent, albeit with a different temporal profile. While the effect of Iso occurred within a few minutes, MMF and Keta/Xyl operated on a longer timescale (Fig. 1E). Moreover, periods of activity were consistently and strongly reduced immediately under Iso and MMF, but delayed by 30 min under Keta/Xyl (Fig. 1F). These results indicate that all anesthetics shift the LFP to lower frequencies and the E/I balance towards inhibition, albeit with different temporal profiles.

In contrast to Keta/Xyl-anesthesia, Isoflurane- and MMF-anesthesia can be efficiently antagonized by removing the face mask or injecting a wake-up cocktail (Flumazenil, Atipamezol and Buprenorphine, FAB) (Albrecht et al., 2014; Fleischmann et al., 2016), respectively. 20-30 min after Iso withdrawal, animals regained motility and periods of silence in the LFP receded (Fig. 1C,F). However, in contrast to post-Iso, LFP power did not fully recover after FAB, remaining significantly reduced at frequencies below 0.5 and above 30 Hz for the entire 45 min-post anesthesia recording period (Fig. 1C,D). In contrast, elevated LFP power in the 0.5-4 Hz band and reduction in active periods remained significant throughout the entire recording in the presence of Keta/Xyl. In line with these results, the 1/f slope promptly reverted to values similar to baseline after Iso discontinuation. In contrast, the recovery was only transitory and partial after MMF antagonization, and virtually absent for Keta/Xyl (Fig. 1E), indicating that the E/I balance recovered only after Iso within 45 min.

Cross-frequency coupling between theta and gamma oscillations has been suggested to underlie information transfer in the hippocampus (Canolty and Knight, 2010). Given the strong decrease of theta power in the presence of Iso and MMF, we reasoned the phase modulation of the gamma rhythm could also be altered. To test this, we used phase-amplitude coupling (PAC) to measure whether the phase of slow LFP oscillations modulates the amplitude of the signal at a higher frequency. In line with previous results (Scheffer-Teixeira et al., 2012; Schomburg et al., 2014) a significant coupling between theta and gamma frequency bands, as well as between frequencies in the 1-2 Hz range and gamma was present in the awake state (Fig. 1G). Moreover, anesthesia strongly altered PAC. In accordance with the LFP power analysis, the coupling reached a maximum strength between the dominant slow-frequency oscillations induced by the various anesthetics (<0.5 Hz for isoflurane, ~1 Hz for MMF and 0.5-4 Hz for Keta/Xyl) and gamma (Fig. 1G). For all anesthetics, the range of phase-modulated amplitudes was wide, suggesting that the modulating phase corresponds to the identified slow-wave activity.

Taken together, these data show that all three GAs differently and persistently modulated the network oscillations in dCA1, a full recovery of activity being detected within 45 min only for Iso.

bioRxiv preprint doi: https://doi.org/10.1101/2020.06.05.135905; this version posted June 6, 2020. The copyright holder for this preprint (which was not certified by peer review) is the author/funder. All rights reserved. No reuse allowed without permission.

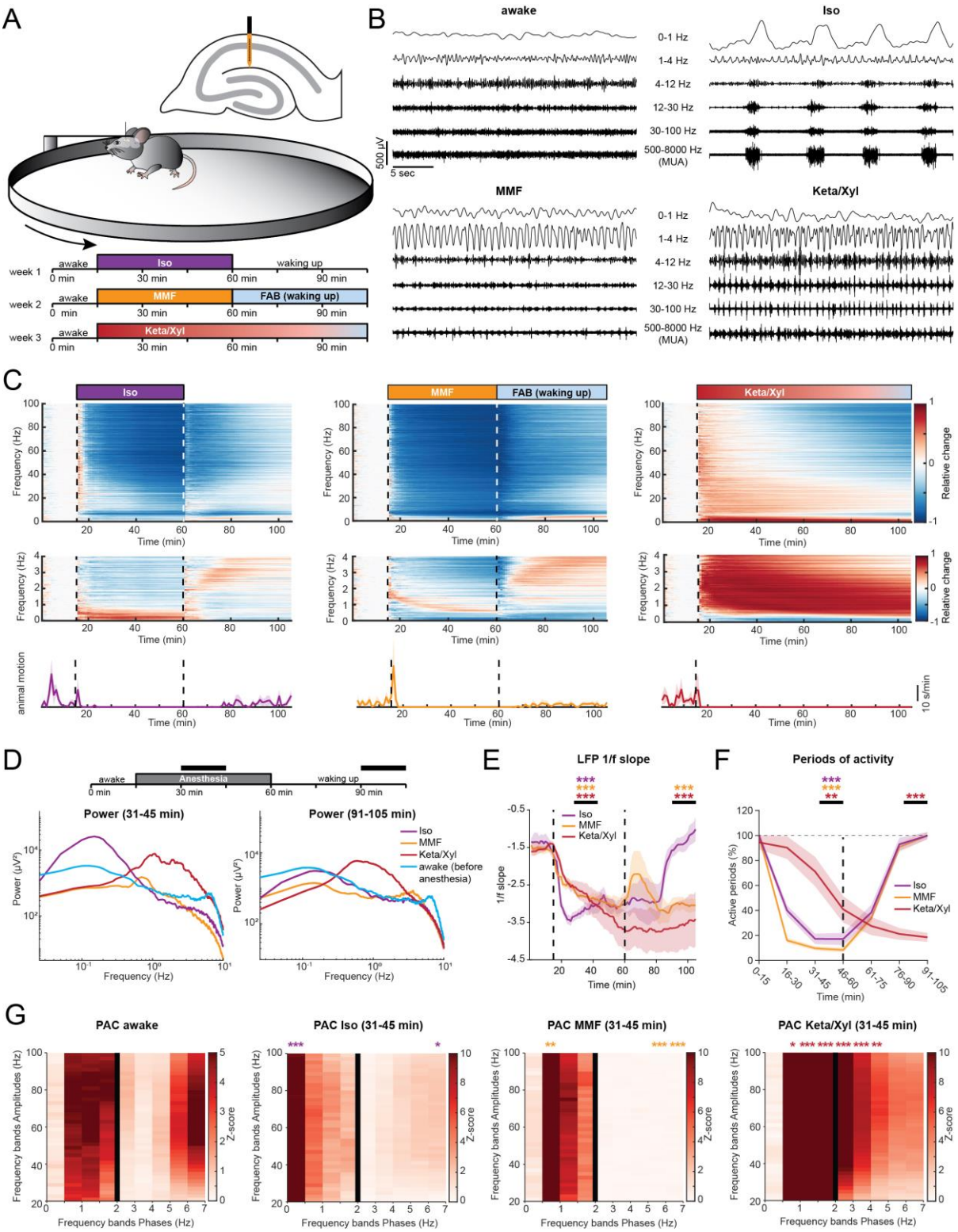

Figure 1: LFP recordings in dorsal CA1 during wakefulness and anesthesia reveal distinct and complex alterations by Iso, Keta/Xyl and MMF. (A) *Experimental setup. Extracellular electrical recordings in dorsal CA1 were performed in four head-fixed mice for 105 min, continuously. Each animal was recorded under all anesthesia as indicated in the scheme. Order of anesthetics was pseud-randomized.* ***(B)*** *Characteristic local field potential (LFP) recordings during wakefulness and under three different anesthetics.* ***(C)*** *Color-coded modulation index (MI) plots (upper and middle panels) for LFP power and motion profiles (lower panels) for the three different anesthetic conditions. Upper panels display LFP power for 0-100 Hz frequency range, lower panels for 0-4 Hz.* ***(D)*** *Line plot displaying LFP power spectra for the two time periods indicated by horizontal black bars. For comparison, the 15-min*

bioRxiv preprint doi: https://doi.org/10.1101/2020.06.05.135905; this version posted June 6, 2020. The copyright holder for this preprint (which was not certified by peer review) is the author/funder. All rights reserved. No reuse allowed without permission.

spectrum of the awake period before anesthesia induction is plotted in both graphs. Statistical differences are indicated in Fig. S1C ***(E)*** *Line plot displaying the power law decay exponent (1/f) of the LFP power spectrum for the 30-50 Hz range. Lines display mean ± SEM.* ***(F)*** *Line plot displaying the fraction of active periods compared to the pre-anesthetic wakeful state, in 15 min bins throughout the entire recording duration. Lines display mean ± SEM.* ***(G)*** *Heat map displaying Phase-amplitude-coupling (PAC) for pre-anesthetic wakeful state (left) and for the indicated time periods during anesthesia. Different bin sizes (0.5 Hz and 1 Hz, separated by vertical black line) are used to resolve low- and high-frequency PAC. Vertical dashed lines in (C) and (E) indicate time points of anesthesia induction (Iso, MMF, Keta/Xyl) and reversal (Iso & MMF only). Vertical dashed line in (F) indicates time point of anesthesia reversal (Iso & MMF only). Asterisks in (E) and (F) indicate significance of time periods indicated by black horizontal line compared to 15-min period before anesthesia. Anesthetic conditions are color-coded. Asterisks in (G) indicate significant differences compared to the corresponding frequency band during wakefulness. * $p < 0.05$, ** $p < 0.01$, *** $p < 0.001$, $n = 4$ mice. For full report of statistics, see statistics table.*

Delayed recovery of neuronal spiking patterns after anesthesia

While the LFP provides information about general network states in the hippocampus, it is influenced by long-range activity and highly active regions in the vicinity of CA1 (Buzsaki et al., 2012). To assess the effects of GAs on CA1 neurons, we analyzed the spiking of individual units (56-72 units per animal, n=4 mice) before, during and after each of the anesthetic conditions. All anesthetics significantly and rapidly (<1 min) decreased spiking activity in CA1 neurons (Fig. 2A,B, S2), with MMF leading to the most potent suppression, followed by Iso and Keta/Xyl. Although the bulk spike rate was strongly reduced, the number of active neurons (see Methods) was only mildly affected (Fig. 2C), reaching a significant reduction only with MMF. This observation suggests that anesthesia broadly reduces neuronal activity, and does not modulate only a discrete subpopulation of neurons. Both firing rate and the number of active neurons recovered within 45 min after reversal for MMF and Iso (Fig. 2A-C, S2).

To investigate whether the rhythmicity of single neuron firing was affected similarly to the LFP, we analyzed the spectral properties of 1 ms-binned SUA firing (i.e. power of SUA spike trains, for details see Methods). In the presence of Iso, SUA power was consistently increased in the range between 0 and 0.5 Hz (Fig. 2A,D, S2), in line with the strong modulation of LFP at 0.1-0.2 Hz. Of note, this effect did not vanish after Iso removal, suggesting that Iso has a long-lasting impact on firing rhythmicity. In contrast, and in line with its effects on the LFP, MMF generally reduced, albeit less strongly, SUA power, including the low frequencies. A significant reduction of SUA power was still present 45 min after antagonization in the 0-0.5 Hz band. Keta/Xyl, on the other hand, only showed a tendency towards reduced SUA power in the frequency band below 0.5 Hz, but increased SUA power significantly in the range between 0.5 and 4 Hz, consistent with its effect on the LFP (Fig. 2D). This modulation was present throughout the entire recording. At higher frequencies, Iso led to a peak in the theta frequency range, similar to wakefulness (Fig. 2E), yet it reduced the SUA power in the beta/gamma range. Keta/Xyl and MMF caused an overall reduction in SUA power at frequencies >5 Hz (Fig. 2E). Thus, GAs differentially impair spiking rhythmicity. These changes appeared to follow similar dynamics than those in the LFP.

To confirm the synchrony between spikes and low-frequency oscillations, we calculated their pairwise phase consistency (PPC) (Vinck et al., 2012). When compared to pre-anesthesia, PPC values for the 0-0.5 Hz frequency band were augmented by Iso. Keta/Xyl increased

bioRxiv preprint doi: https://doi.org/10.1101/2020.06.05.135905; this version posted June 6, 2020. The copyright holder for this preprint (which was not certified by peer review) is the author/funder. All rights reserved. No reuse allowed without permission.

coupling of spikes to the LFP between 0.5 and 1 Hz, whereas MMF showed a weak, but significant increase of coupling at frequencies below 1 Hz (Fig. 2F).

Similar to the LFP, the SUA firing rate nearly fully recovered during the 45 min post-Iso (Fig. 2A,B, S2), with even a slight, but significant increase at the end of the recording period. In contrast, after FAB-induced MMF reversal, CA1 spiking activity remained slightly reduced, reflecting the lack of LFP recovery. For Keta/Xyl, SUA remained suppressed during the entire recording period (Fig. 2B). Strikingly, SUA power did not fully recover for any of the tested anesthetics (Fig. 2E).

Taken together, we show that all investigated GAs caused a persistent and robust reduction of CA1 firing. Moreover, spiking during anesthesia was phase-locked to the GA-induced slow network oscillations.

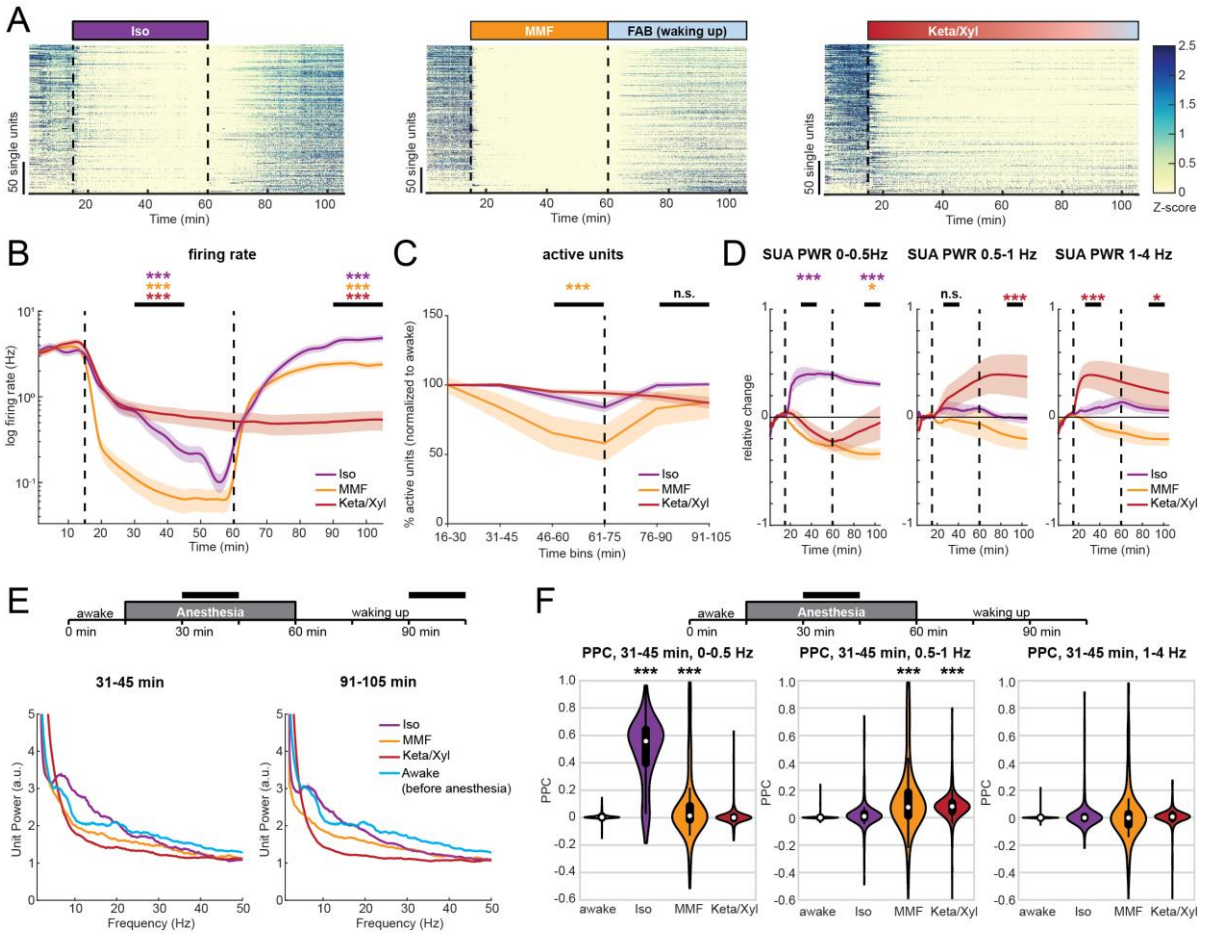

Figure 2: Single unit activity in dorsal CA1 is strongly reduced during anesthesia, and remains significantly altered long after its termination. (A) *Raster plots of z-scored single-unit activity (SUA) for the three different anesthetic strategies in four mice. Units are sorted according to initial activity during wakefulness.* ***(B)*** *Line plot of SUA firing rate before, during and after anesthesia induction.* ***(C)*** *Line plot displaying the fraction of active units compared to the pre-anesthetic wakeful state, for all three anesthetics in 15 min bins throughout the entire recording duration.* ***(D)*** *Relative change of population firing rate power in the 0-0.5, 0.5-1 and 1-4 Hz frequency band. SUA PWR = power of SUA spike trains.* ***(E)*** *Line plot displaying the normalized power spectra of population firing rate for the two time periods indicated by horizontal black bars. For comparison, the 15-min spectrum for pre-anesthetic wakeful state is plotted in both graphs.* ***(F)*** *Pairwise phase consistency (PPC) at low frequencies in the same frequency bands as (D), for the indicated time points during anesthesia. White dots indicate median, vertical thick and thin lines indicate 1st-3rd quartile and interquartile range, respectively. Colored lines in (B) - (D)*

bioRxiv preprint doi: https://doi.org/10.1101/2020.06.05.135905; this version posted June 6, 2020. The copyright holder for this preprint (which was not certified by peer review) is the author/funder. All rights reserved. No reuse allowed without permission.

*display mean ± SEM. Vertical dashed lines in panels (A), (B) and (D) indicate time points of anesthesia induction (Iso, MMF, Keta/Xyl) and reversal (Iso & MMF only). Vertical dashed line in (C) indicates time point of anesthesia reversal (Iso & MMF only). Asterisks in (B) - (D) indicate significance of time periods indicated by black horizontal line compared to period before anesthesia. Anesthetic conditions are color-coded. Asterisks in (F) indicate significant differences to wakefulness. * $p < 0.05$, ** $p < 0.01$, *** $p < 0.001$, $n = 4$ mice. For full report of statistics, see statistics table.*

Iso, Keta/Xyl and MMF reduce number, amplitude, and duration of calcium transients

To monitor the population dynamics of CA1 neurons in the presence of different anesthetics, we imaged the same field of view (FOV) using the genetically encoded indicator GCaMP6f (Chen et al., 2013) and systematically compared the activity of identified neurons during quiet wakefulness and in the presence of different anesthetics (Fig. 3A).

First, we considered all active neurons in each condition and analyzed the average rate (i.e., the number of transients), amplitude, and duration (i.e., the decay constant) of calcium transients across all imaging sessions in 7 mice. In line with the results of SUA analysis (see Fig. 2C), a large number of CA1 pyramidal neurons were active in the presence of all three GAs. Using extraction parameters that restricted the number of ROIs but maximized signal quality (see Methods), we obtained a median of 311 (min-max of 16-817) active neurons per FOV, for a total of 189 five-minutes recordings. All GAs significantly altered calcium dynamics in CA1 neurons, reducing the activity (Fig. 3C,D), as previously shown for neuronal spiking (Fig. 2B). However, each condition could be characterized by a specific signature in their calcium dynamics. Iso yielded only a mild decrease of rate and amplitude, but a strong reduction of duration of calcium transients (Fig. 3D). Consistent with effects on LFP and SUA, calcium transients showed a spectral peak between 0.1 and 0.2 Hz (Fig. S4). In contrast to Iso, MMF did not significantly affect the duration of transients but reduced their rate and amplitude when compared to wakefulness. Keta/Xyl-anesthesia had the strongest effect on calcium transients, leading to a reduction of all three parameters compared to wakefulness (Fig. 3D). Unlike for electrophysiological recordings, no spectral peak was present in calcium transients, most likely due to the strong suppression of calcium activity by Keta/Xyl. Considering all parameters, the four groups tended to segregate into clusters, one consisting mostly of recordings under Keta/Xyl, and another one consisting of awake and Iso recordings. Most recordings under MMF clustered between these two groups (Fig. 3E). Importantly, these findings were robust to changes in the signal extraction pipeline. Varying the threshold for calcium transient detection across a wide range of values did not affect the reported effects on rate and height of transients (Fig. S3B). Further, conducting the same analysis on neuronal activity metrics that are independent of calcium transients detection (integral and standard deviation) or on dF/F calcium signals also yielded analogous results (Fig. S3C-E).

bioRxiv preprint doi: https://doi.org/10.1101/2020.06.05.135905; this version posted June 6, 2020. The copyright holder for this preprint (which was not certified by peer review) is the author/funder. All rights reserved. No reuse allowed without permission.

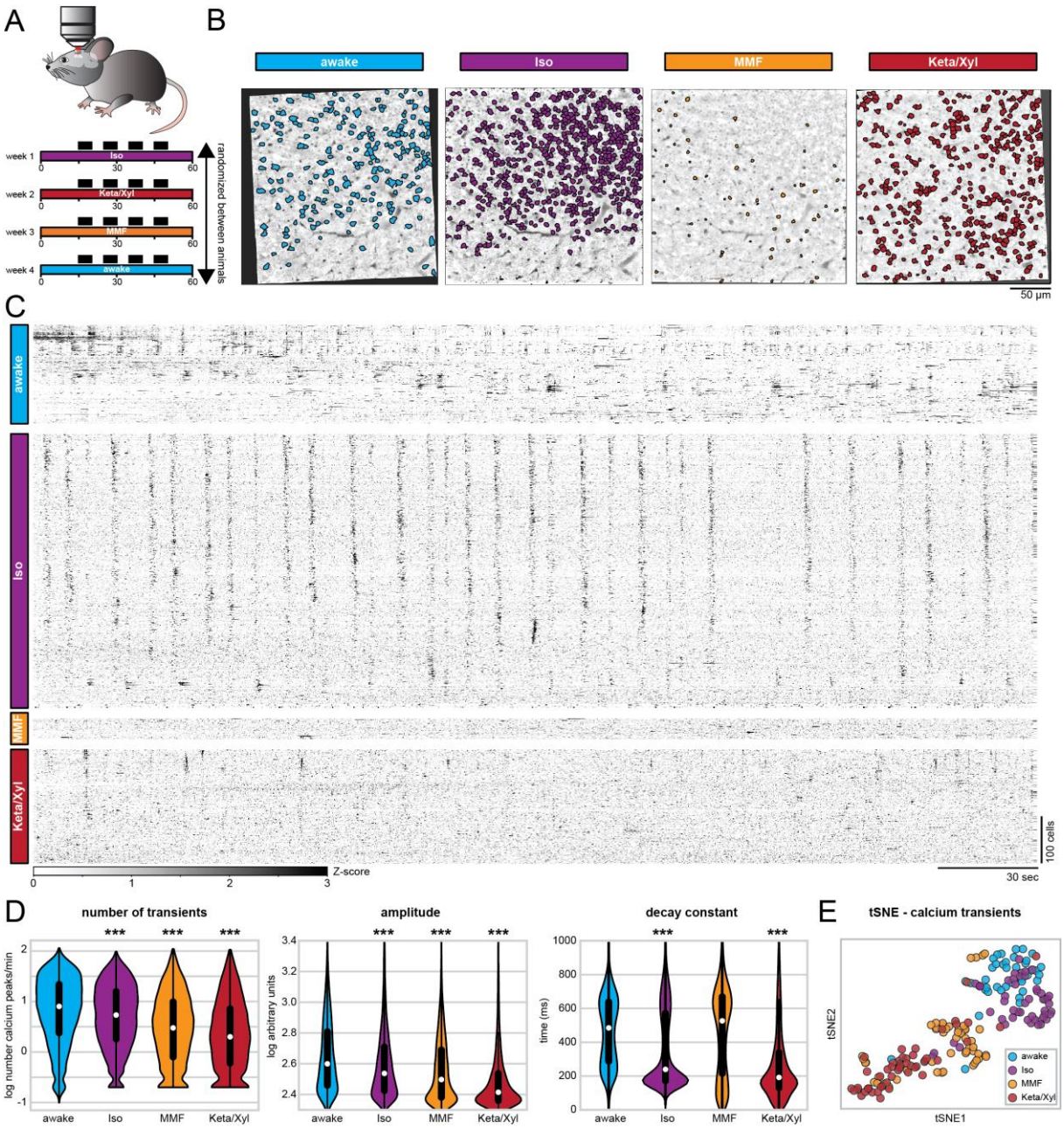

Figure 3: Repeated calcium imaging in dorsal CA1 reveals distinct activity profiles for Iso, MMF and Keta/Xyl. (A) *Experimental strategy for chronic calcium imaging of cellular activity in dorsal CA1. For each condition, mice were imaged four times for five minutes in seven mice, as indicated by black fields in the scheme. The order of imaging conditions was pseudo-randomized.* ***(B)*** *Time-averaged, two-photon images of the same FOV in CA1 aligned to the Iso condition. ROIs of automatically extracted, active neurons are overlaid for each condition.* ***(C)*** *Raster plots of z-scored calcium transients in the same animal under different conditions. Traces are sorted by similarity.* ***(D)*** *Violin plots quantifying the number (left), amplitude (middle), and decay (right) of detected calcium transients. White dots indicate median, vertical thick and thin lines indicate 1st-3rd quartile and interquartile range, respectively.* ***(E)*** *tSNE plot summarizing the average calcium transients properties. Each data point represents one recording session. Asterisks in (D) indicate significant differences to wakefulness. *** $p < 0.001$. Note, to facilitate readability, only differences to wakefulness are indicated. For full report of statistics, see statistics table.*

bioRxiv preprint doi: https://doi.org/10.1101/2020.06.05.135905; this version posted June 6, 2020. The copyright holder for this preprint (which was not certified by peer review) is the author/funder. All rights reserved. No reuse allowed without permission.

Iso, Keta/Xyl and MMF distinctly modulate cellular calcium dynamics in a given neuron

One possible explanation for these distinct modes of calcium activity could be that each anesthetic condition recruits a unique set of neurons characterized by particular spiking properties. We tested this possibility by analyzing calcium transients in neurons that were active during all conditions (Fig. 4A, S5, S6). To obtain a sufficient number of active neurons, we extracted calcium transients using a lower quality threshold, accepting more neurons per recording (see Methods). In this manner, we obtained a median of 783 neurons per recording (min-max of 156-1641). While this shifted the overall distribution of calcium parameters to lower values, the relative ratios between the four conditions remained the same and the differences between anesthesia groups were preserved (Fig. S3F-G). Also, when considering only neurons that were active in all four conditions, rate as well as amplitude of calcium peaks were generally reduced under anesthesia being lowest in the Keta/Xyl condition (Fig. 4B,C). Compared to the whole dataset, differences in decay constant were less pronounced. The median decay constant strongly decreased for awake and MMF conditions, while it increased for Iso and Keta/Xyl. These results indicate that both the between- as well as the within-condition variance strongly decreased when considering only neurons active under all conditions.

The relatively low number of neurons active in all four conditions (335 neurons) limited the statistical analysis. Therefore, we additionally compared neurons that were active in any two combinations of conditions (Fig. S7). This analysis further corroborated the similarity of neurons active during wakefulness and Iso anesthesia (Fig. 4C, S7). Rate, amplitude, and duration of calcium transients were most similar between wakefulness and Iso compared to the other GAs. In contrast, neurons active during wakefulness and either Keta/Xyl or MMF showed decreased rate, amplitude and duration under anesthesia, with Keta/Xyl causing the strongest phenotype (Fig S7). Overall, this indicates that anesthetics influence the firing properties of hippocampal neurons. However, the magnitude and the direction of these effects vary considerably. Iso anesthesia has the mildest effect, and it most likely arises from distinct neuronal populations being active in the two conditions (wakefulness vs. Iso anesthesia), as the firing properties of cells that are active in both are barely affected (Fig. 4B,C). On the other hand, the strong effects of MMF and Keta/Xyl on all calcium parameters in the same cells indicate that different anesthetics directly alter the firing properties of individual neurons. Thus, alterations in firing properties of neuronal populations (e.g. SUA, Fig. 2B-D) are not solely explainable by different subpopulations of neurons being active between awake and anesthesia.

bioRxiv preprint doi: https://doi.org/10.1101/2020.06.05.135905; this version posted June 6, 2020. The copyright holder for this preprint (which was not certified by peer review) is the author/funder. All rights reserved. No reuse allowed without permission.

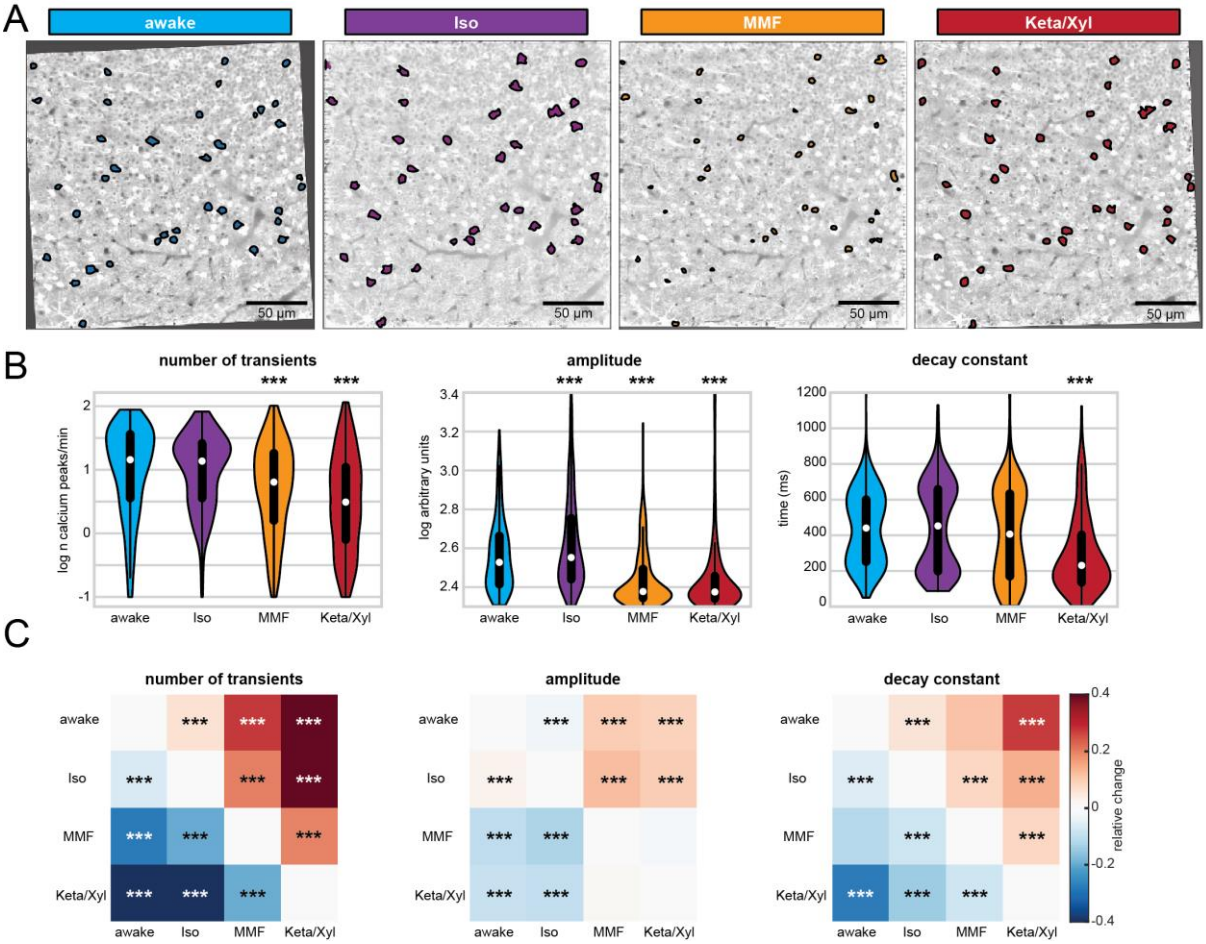

Figure 4: Calcium activity profiles in neurons active during all conditions are similar between wakefulness and Iso. (A) *Two-photon time-averaged images of the same FOV in CA1, aligned to the Iso condition (same images as in figs. 3). ROIs show neurons that were active in each condition, allowing direct comparison of calcium transients in the same cells under different conditions.* ***(B)*** *Violin plots quantifying the number (left), amplitude (middle), and decay (right) of detected calcium transients. White dots indicate median, vertical thick and thin lines indicate 1st-3rd quartile and interquartile range, respectively.* ***(C)*** *Heat maps displaying the relative change in the number (left), amplitude (middle), and decay (right) of calcium transients between neurons active in pairs of conditions (see also Fig. S7). Asterisks in (B) and (C) indicate significant differences to wakefulness. *** $p < 0.001$. Note, to facilitate readability, only differences to wakefulness are indicated. For full report of statistics, see statistics table.*

Anesthesia decorrelates hippocampal activity

Calcium imaging studies in the visual cortex of ketamine anesthetized rats (Greenberg et al., 2008) and isoflurane anesthetized mice (Goltstein et al., 2015) showed that anesthesia increases the overall pairwise correlations between firing neurons, and consequently, induces more structured patterns of activity in the neocortex. While neocortical L2/3 cells typically show a high degree of local interconnectivity (Harris and Mrsic-Flogel, 2013), this is not the case for CA1, where pyramidal cells receive their main excitatory input from CA3 and entorhinal cortex and send their efferents to subiculum and extrahippocampal areas (Neves et al., 2008). Another difference between neocortex and hippocampal CA1 area is that the neocortex receives strong direct input from primary thalamus, which is a major source for slow oscillations during anesthesia-induced unconsciousness and sleep (Franks, 2008; Klinzing et al., 2019; Rudolph and Antkowiak, 2004). In comparison to neocortex, hippocampus shows different

bioRxiv preprint doi: https://doi.org/10.1101/2020.06.05.135905; this version posted June 6, 2020. The copyright holder for this preprint (which was not certified by peer review) is the author/funder. All rights reserved. No reuse allowed without permission.

patterns of activity, including sharp waves, which are generated intrinsically in the hippocampus, likely originating in CA3 (Buzsaki, 1986). To investigate whether these differences cause a different impact of anesthesia on the population activity in CA1 when compared to the neocortex, we analyzed the dynamical structure of population activity using both calcium imaging and SUA of extracellular recordings in vivo. First, we analyzed Fisher-corrected Pearson pairwise correlation between neuropil-corrected, raw fluorescence traces. We found that both correlation and anticorrelation were highest in animals during quiet wakefulness (Fig 5A-B). In particular, the awake condition had a higher proportion of correlation coefficients both in the 1st as well as in the 4th quartile of the entire distribution and, accordingly, higher absolute correlation values (Fig. 5B, S8A). Similar to the firing properties, Iso induced the milder changes, whereas Keta/Xyl caused the strongest phenotype. This relationship was preserved in neurons active during all conditions (Fig. S8B), indicating that anesthesia generally reduces correlated activity between neurons and that this effect is not attributable to the activity of particular neuronal subpopulations. Moreover, these effects were not influenced by the distance between the pair of neurons whose correlation was quantified (Fig. 5C). These findings highlight the major differences between the anesthesia-induced effects on neuronal coupling in hippocampal CA1 and neocortex. In accordance with the anatomy of CA1, the correlation between pairs of neurons was only mildly affected by the distance between them, with or without anesthesia. Not only were neurons less highly correlated to each other under anesthesia, but their coupling to the whole population activity (Okun et al., 2015) was reduced as well. The proportion of neurons with population coupling in the 4th quartile of the entire distribution was highest for awake, and most strongly reduced under Keta/Xyl and MMF, while Iso showed only mild effects (Fig. 5D).

To further relate the calcium imaging data to extracellular recordings of neuronal firing, we carried out an analogous analysis on SUA. To avoid the confounding effect of firing rate, we quantified the correlation between pairs of neurons using the Spike-Time Tiling Coefficient (Cutts and Eglen, 2014), a measure that is largely insensitive to variations of the firing rate (see Methods). To be consistent with the calcium data, we quantified correlations within 1 second, a timescale of the same magnitude as the decay constant used to extract calcium signals (700 ms). This analysis confirmed that all anesthetics decorrelated neuronal activity (Fig. 5E). This effect was still present, albeit less strongly pronounced, using an integration window of 10 ms, which is closer to the duration of electrically measured spikes (Fig. S9). Overall, the decorrelation was milder under Iso anesthesia and stronger under Keta/Xyl and MMF. Thus, all three GAs decorrelated calcium transients and spiking activity in the CA1 area, with MMF and Keta/Xyl inducing the most prominent effects.

bioRxiv preprint doi: https://doi.org/10.1101/2020.06.05.135905; this version posted June 6, 2020. The copyright holder for this preprint (which was not certified by peer review) is the author/funder. All rights reserved. No reuse allowed without permission.

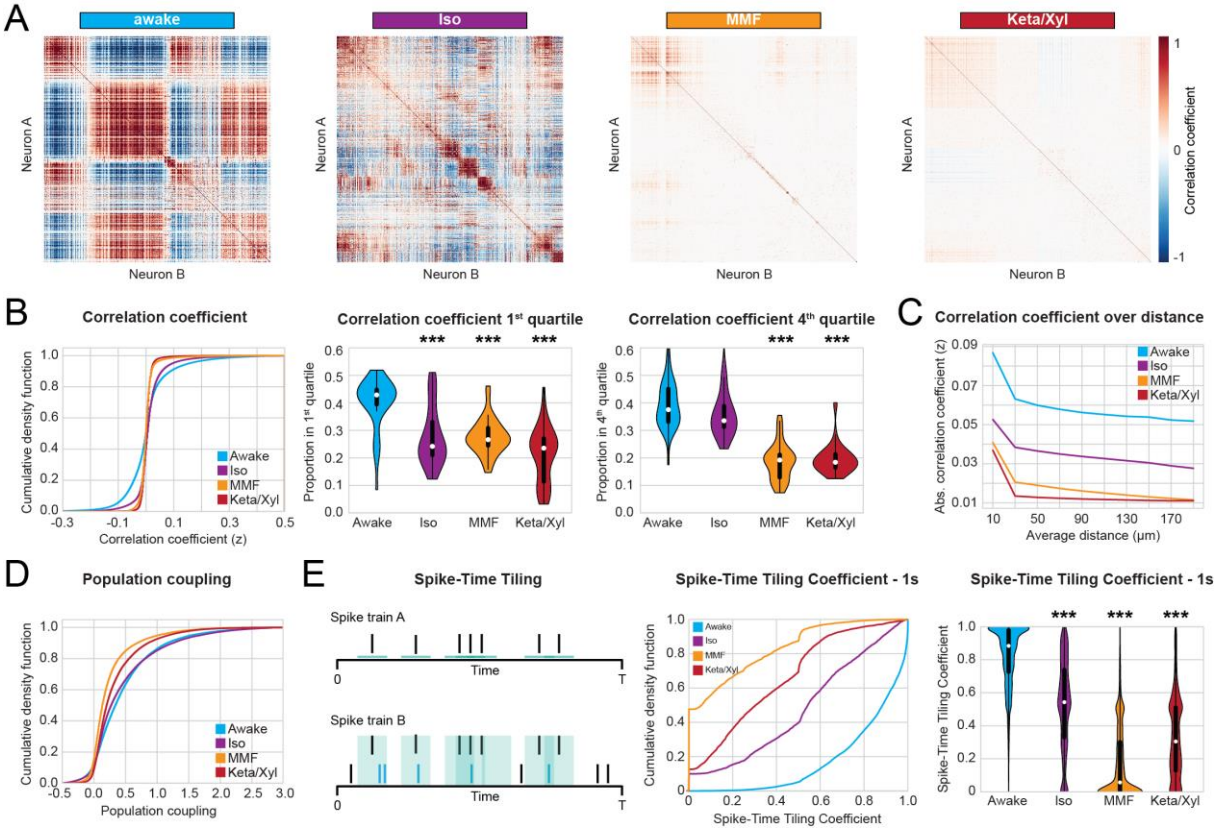

Fig. 5. Correlation analysis of CA1 calcium and spiking shows decorrelation under anesthesia. ***(A)*** *Heat maps displaying representative correlation matrices between pairs of neurons during wakefulness and the three different anesthetic conditions, in the same animal. Matrices are sorted by similarity.* ***(B)*** *Left: Line plot displaying cumulative distribution of Fisher-corrected Pearson correlation coefficients between pairs of neurons. Center: violin plot displaying the proportion of pairs found in the 1st (most negative) and 4th (most positive) quartile of the distribution.* ***(C)*** *Line plot displaying the absolute pairwise correlation coefficients over distance (25 micrometer bins).* ***(D)*** *Line plot displaying cumulative distribution of population coupling.* ***(E)*** *Quantification of correlation between pairs of extracellularly recorded single units using the Spike-Time Tiling Coefficient (STTC). Left: Schematic illustration of the STTC quantification. Center: cumulative distribution of the STTC with a 1000 ms integration window. Right: violin plot quantifying the STTC. In violin plots, white dots indicate median, vertical thick and thin lines indicate 1st-3rd quartile and interquartile range, respectively. Asterisks in (B) and (E) indicate significant differences to wakefulness. *** $p < 0.001$. Note, only differences to wakefulness are indicated. For comparison between conditions, see statistics table.*

Anesthesia fragments temporal and spatial structure of hippocampal activity

The decorrelation of neuronal activity during anesthesia suggests that GAs might impact the spatial and temporal organization of CA1 neuronal ensembles (see Fig. 5A). To test this hypothesis, we analyzed the same number of active neurons for each condition, since a different number of neurons in each condition potentially influences the number and size of detected clusters (Wenzel et al., 2019). First, we monitored the impact of GAs on the temporal structure of CA1 activity. We defined the number of clusters identified by principal component analysis (PCA) as the number of components that were needed to explain 90% of the variance. Moreover, we assessed the power-law slope of variance explained over the first 150 components (Fig. 6A). Both methods led to a larger number of clusters and a flatter power-law slope for anesthesia when compared to wakefulness (Fig. 6A). Further corroborating these

bioRxiv preprint doi: https://doi.org/10.1101/2020.06.05.135905; this version posted June 6, 2020. The copyright holder for this preprint (which was not certified by peer review) is the author/funder. All rights reserved. No reuse allowed without permission.

findings, both tSNE dimensionality reduction and affinity propagation (AP) clustering (see Methods) also revealed a larger number of clusters for anesthesia compared to wakefulness (Fig. 6B,C). These observations indicate that activity is less structured under anesthesia. In line with previous results, Iso had the weakest effect, whereas Keta/Xyl consistently induced the most pronounced phenotype. Analysis on the deconvolved calcium traces led to comparable results (Fig S10A,B). These findings support the idea that GAs cause a fragmentation of the network consisting of a more diverse repertoire of microstates.

Second, we tested whether anesthesia disrupted the spatial structure of hippocampal activity, employing a modularity maximization approach (Newman and Girvan, 2004; Sporns and Betzel, 2016) designed to detect internally densely connected communities (modules). To allow detection of modules at varying sizes, we carried out our analysis while varying a resolution parameter (gamma) and thus focusing on different spatial scales. Using this approach, we showed that GAs increase the number of detected communities over a wide range of resolution parameter values (Fig 6D). Moreover, the modularity of these communities was lower than in wakefulness (Fig 6E). These results indicate that anesthesia results in a more fractured network with, on average, smaller and less coherent communities. A multi-resolution approach (Jeub et al., 2018) followed by the selection of partitions based on hierarchical consensus clustering yielded similar results (Fig. S10C). Among GAs, Iso induced the mildest phenotype, whereas Keta/Xyl had the most prominent effects. Thus, GAs not only decorrelate hippocampal activity, but also consistently fragment both its temporal and spatial structure.

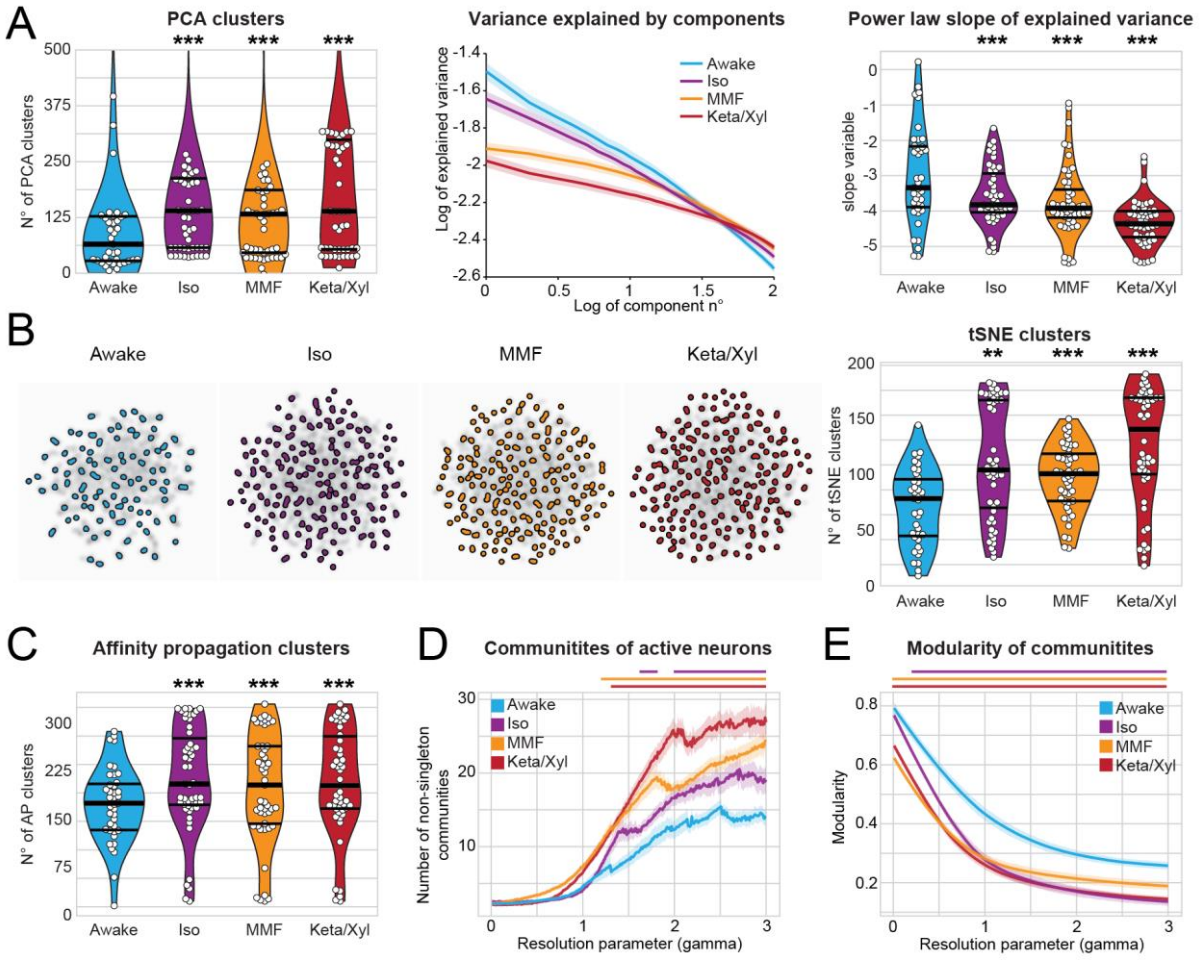

bioRxiv preprint doi: https://doi.org/10.1101/2020.06.05.135905; this version posted June 6, 2020. The copyright holder for this preprint (which was not certified by peer review) is the author/funder. All rights reserved. No reuse allowed without permission.

Fig. 6. Calcium activity in CA1 is temporally and spatially fragmented during anesthesia. (A) *Left: violin plot quantifying the number of principal component analysis (PCA) clusters during wakefulness or anesthesia, as indicated. Middle: loglog line plot displaying the variance explained by the first 100 components for each condition. Right: violin plot quantifying the power-law slope of the variance explained by the first 100 components for each condition.* ***(B)*** *Left: tSNE plots of network events recorded in the same animal under the four indicated conditions. Right: Violin plot quantifying the number of tSNE clusters obtained from calcium recordings during the four different treatments.* ***(C)*** *Violin plot quantifying the number of clusters obtained by affinity propagation from calcium recordings during the four different treatments.* ***(D)*** *and* ***(E)*** *Line plots quantifying the number of detected communities and the modularity of the detected communities with the resolution parameter gamma ranging from 0 to 3. Horizontal lines in violin plots indicate median and 1st-3rd quartile. Asterisks in (A) - (C) indicate significant differences to wakefulness. ** $p < 0.01$, *** $p < 0.001$. Horizontal lines above plots in (D) - (E) indicate significant difference to wakefulness. Anesthetic conditions are color-coded. Note, only differences to wakefulness are indicated. For comparison between conditions, see statistics table.*

Repeated anesthesia alters spine dynamics in CA1

The impact of Iso, MMF, and Keta/Xyl on CA1 activity might alter spine dynamics at CA1 pyramidal neurons. This issue is of critical relevance, since GAs disrupt activity patterns during development (Chini et al., 2019) also involving alteration of synaptic connectivity (Briner et al., 2010; Briner et al., 2011; De Roo et al., 2009), but less is known about the impact of GAs on hippocampal synaptic structure during adulthood. So far, spine dynamics in hippocampus were only investigated under anesthesia, lacking comparison to the wake state. Moreover, the reported turnover rates varied strongly between studies (Attardo et al., 2015; Gu et al., 2014; Pfeiffer et al., 2018). Thus, it is unknown how repeated anesthesia in itself affects spine stability.

We repeatedly imaged the same basal, oblique, and tuft dendritic segments of CA1 pyramidal neurons under all four conditions (five times per condition, every four days), interrupted by a 30-day recovery period between conditions (Fig. 7A, S11A). To rule out time-effects, we pseudo-randomized the order of anesthetics (Fig. S11A). During wakefulness, without any anesthesia in between, the turnover ratio of spines on all dendrites was on average 18.6 - 20.5 % per four days. This turnover ratio was stable and did not change systematically over successive imaging sessions (Fig. 7B). Notably, all anesthetics affected spine turnover. Both MMF and Iso anesthesia mildly increased the turnover ratio compared to wakefulness (21.1 – 23.8 % for MMF, 24.0 – 24.7 % for Iso). Iso did not alter the surviving fraction of spines. Together with the significant increase in spine density over time (Fig. 7B) these results indicate that the elevated turnover ratio was due to a rise in the gained fraction of spines (Fig. S11B). In contrast, MMF led to a slight increase in the fraction of lost spines (Fig. S11B) and correspondingly, slightly decreased the surviving fraction compared to wakefulness. Spine density did not change over time. Keta/Xyl anesthesia showed the strongest effect on spine turnover (13.4 - 15.7 %), which was opposite to MMF and Iso, and therefore significantly lower rather than higher compared to the awake condition (Fig. 7B). This lower turnover ratio was accompanied by a higher surviving fraction and an increase in density with time (Fig. 7B). Consistently, the fraction of lost spines was most strongly reduced (Fig. S11B). Thus, Keta/Xyl anesthesia resulted in marked stabilization of existing spines and a reduction in the formation of new spines, indicative of a significant effect on structural plasticity.

To rule out that the age of the animal influenced spine dynamics in the awake condition, we measured spine turnover in a group of age-matched animals to the first anesthesia group (Fig.

bioRxiv preprint doi: https://doi.org/10.1101/2020.06.05.135905; this version posted June 6, 2020. The copyright holder for this preprint (which was not certified by peer review) is the author/funder. All rights reserved. No reuse allowed without permission.

S11A,C). Moreover, to rule out that the chronic imaging procedure per se and anesthesia in general had a long-lasting effect on the awake imaging condition, we added another awake-imaging control group with naïve, age-matched animals to the awake imaging time point in the experimental group (Fig. S11A,C). In all three groups, spine turnover was indistinguishable, indicating that neither age nor previous imaging under anesthesia impacted spine dynamics in the awake-imaging group (Fig. S11C).

Next, we asked whether the modulation of spine turnover by GAs was due to acute remodeling of spines during the time of anesthesia. Alternatively, spine turnover might be driven by long-lasting changes in network activity imposed by the slow reversal of all GAs. To capture fast events such as filopodia formation, we acquired image stacks every 10 min (Fig. 7C). Spine turnover, survival, or density were not significantly altered during the one hour of imaging (Fig. 7D). Thus, spines were stable during the one hour irrespective of the treatment. While mature spines typically show low elimination/formation rates over one hour, filopodia are more dynamic (Dailey and Smith, 1996; Lendvai et al., 2000; Portera-Cailliau et al., 2003). Unlike other reports, that observed an acute selective formation of filopodia under Keta/Xyl, but not Iso (Yang et al., 2011), we did not detect any acute effects of GAs on filopodia turnover of CA1 pyramidal cell dendrites. Thus, chronic exposure to all GAs consistently impacted spine dynamics, whereas acute effects were lacking. Keta/Xyl caused a strong decrease in spine turnover, accompanied by a higher surviving fraction and an increased density over time.

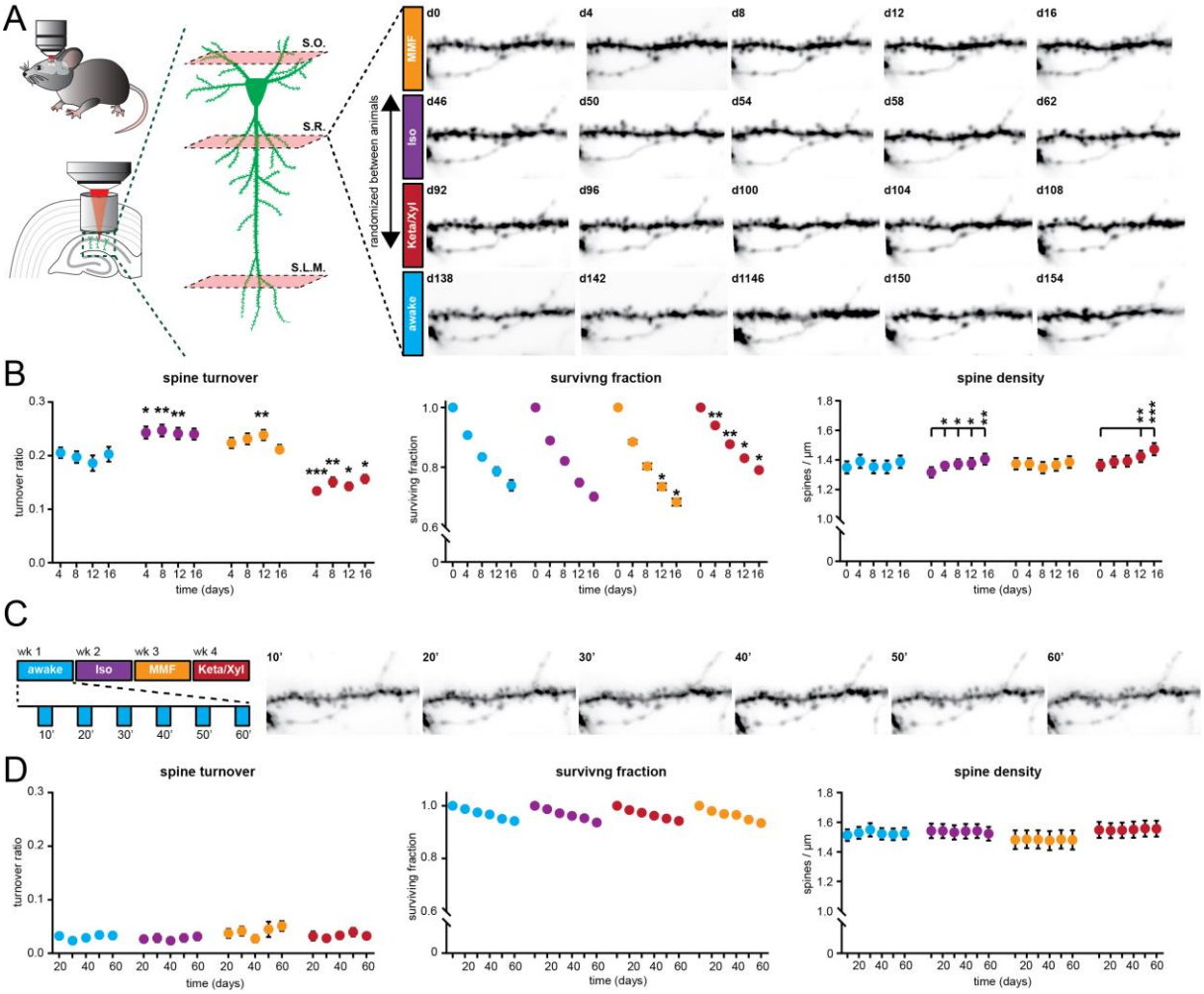

Fig. 7. Spine turnover at CA1 pyramidal neurons is distinctly altered by repeated application of Iso, MMF and Keta/Xyl. (A) *Left: Schematic illustration of in vivo spine imaging strategy. In each animal,*

bioRxiv preprint doi: https://doi.org/10.1101/2020.06.05.135905; this version posted June 6, 2020. The copyright holder for this preprint (which was not certified by peer review) is the author/funder. All rights reserved. No reuse allowed without permission.

spines were imaged on basal dendrites located in stratum oriens (S.O.), oblique dendrites in stratum radiatum (S.R.) and tuft dendrites in stratum lacunosum moleculare (S.L.M.). Right: Example showing an oblique dendrite in S.R. imaged chronically during all conditions. The order of anesthetic treatments was pseudo-randomized between mice (see Fig. S11). ***(B)*** *Dot plots showing quantification of spine turnover (left), spine survival (middle) and spine density (right) under the four indicated treatments. Note that spines were imaged on the same dendrites across all conditions. Dots indicate mean ± SEM. Asterisks indicate significant differences to wakefulness in the left and middle panel. In the right panel, asterisks denote significant changes within each treatment compared to day 0. * $p < 0.05$, ** $p < 0.01$, *** $p < 0.001$.* ***(C)*** *Imaging of acute spine dynamics during four different conditions. Left: schematic of the experimental timeline. Right: example of dendrite imaged during wakefulness in 10 min intervals (same dendrite as in A).* ***(D)*** *Dot plots showing quantification of acute spine turnover (left), spine survival (center) and spine density (right) under the four indicated treatments. Dots indicate mean ± SEM.*

Episodic memory consolidation is impaired by MMF and Keta/Xyl, but not by Iso

Episodic memory formation and consolidation require hippocampal activity. Newly learned experiences are thought of being consolidated via replay events that co-occur with low-frequency oscillations (Klinzing et al., 2019; Moscovitch et al., 2016; Nadel and Moscovitch, 1997; O'Neill et al., 2010). In the hippocampus, these low-frequency events typically occur as sharp waves (Buzsaki, 1986) during sleep, but also during awake resting behavior (O'Neill et al., 2010). The above results from electrophysiological recordings and imaging showed that GAs strongly altered network oscillations in the CA1 area, in the case of MMF and Keta/Xyl, also long after anesthesia discontinuation. Spine turnover of CA1 pyramidal neurons was also affected, especially after Keta/Xyl administration. Therefore, we tested whether inducing anesthesia for 1 hour shortly after the acquisition of a new episodic memory affected its consolidation (Fig. 8A). In line with previous experiments, we restricted Iso and MMF anesthesia to one hour, while Keta/Xyl anesthesia was left to recede spontaneously. We assessed episodic-like memory with a water maze protocol for reversal learning, when the hidden platform was moved to the quadrant opposite the initial target location (Fig. 8A). Specifically, we tested the effects of the different anesthetics on the consolidation of the memory of the new platform location. We compared the performance of the mice during the probe trial done on day 3 immediately after the reversal learning protocol (and 30 min before anesthesia), with the performance during the probe trial on day 4, twenty-four-hours after anesthesia. During the probe trial on day 3, animals of all four groups spent significantly more time in the new target quadrant compared to chance (25 %), indicating that they learned the new platform position successfully (Fig. 8B,C).

On day 4, control animals that did not undergo anesthesia showed the same performance as on day 3, suggesting that they had retained the memory of the new platform location (Fig. 8B,C). However, animals that were anesthetized with Keta/Xyl or MMF spent significantly less time in the new target quadrant and showed a significantly larger mean distance to the target platform position compared to the probe trial on day 3. In the Iso group, no significant difference compared to day 3 was detectable (Fig. 8B,C, S12). Notably, the effects were relatively mild, and the decrease in performance on day 4 was not significantly different between treatment groups. In summary, consistent with long-lasting effects on CA1 network activity, Keta/Xyl, and MMF impaired episodic-like memory consolidation. In contrast, Iso, which overall caused a weaker disturbance of neuronal population activity and a faster recovery profile, did not significantly affect memory consolidation.

bioRxiv preprint doi: https://doi.org/10.1101/2020.06.05.135905; this version posted June 6, 2020. The copyright holder for this preprint (which was not certified by peer review) is the author/funder. All rights reserved. No reuse allowed without permission.

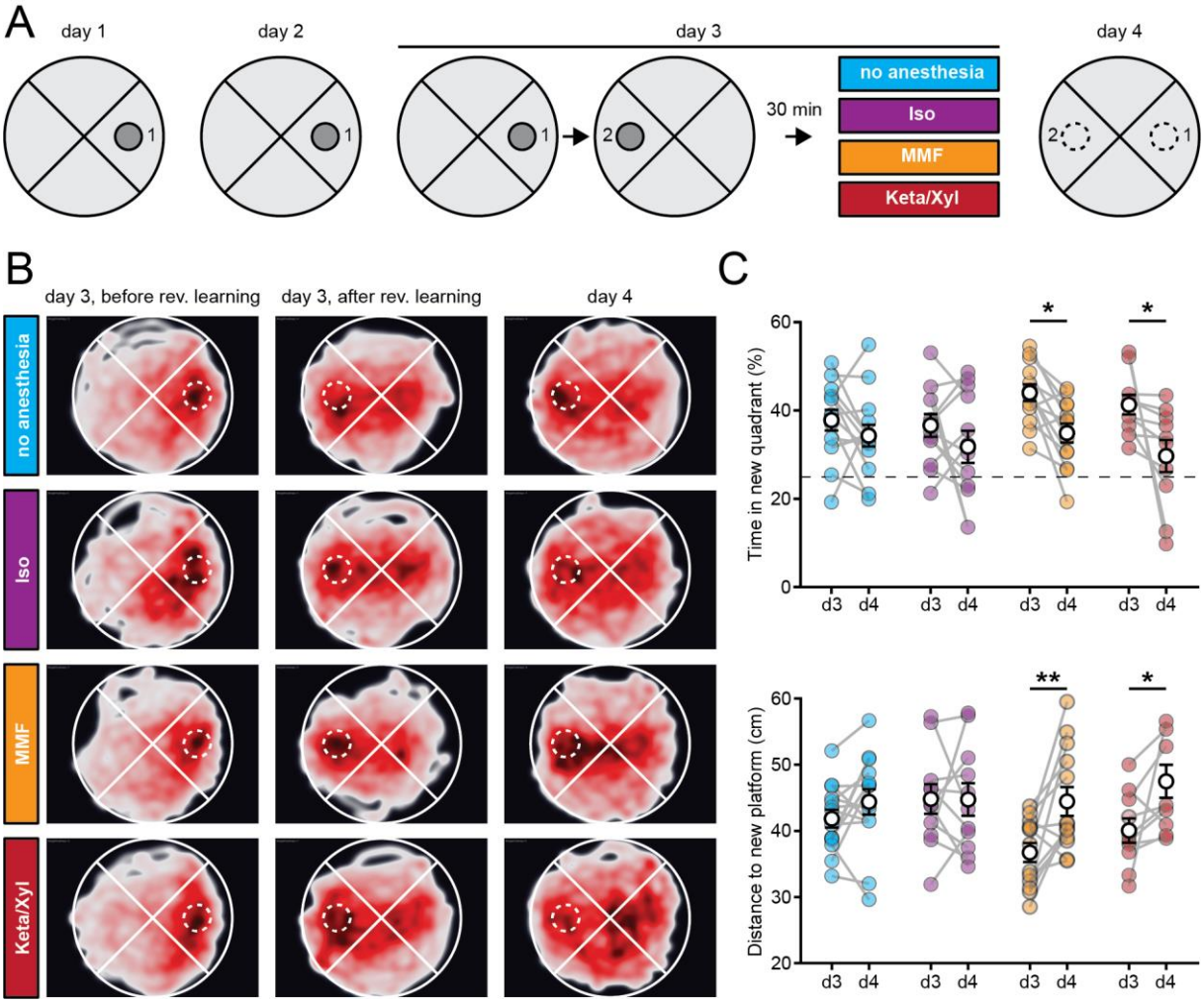

Fig. 8. Episodic memory consolidation is impaired by MMF and Keta/Xyl, but not by Iso. (A) *Experimental design to test episodic-like memory in a Morris water maze. On days 1 and 2 animals were trained to find the platform in position 1. Reversal learning was performed on day 3 where animals had to learn that the platform was moved to position 2. Training was followed 30 min later by a 1-h period of one of the four indicated treatments per group. On day 4, consolidation of the memory for the platform in position 2 was tested.* ***(B)*** *Heat maps showing trajectories of all mice during the first probe trial before reversal learning on day 3 (left column), after reversal learning on day 3 (middle column) and after treatment on day 4 (right column). Position of the target zone is indicated by dashed circles.* ***(C)*** *Scatter plots showing quantification of time spent in the new target quadrant (top) and distance to the new platform (bottom) after reversal learning on day 3 and on day 4. Filled, colored circles indicate individual animals, White circles indicate mean ± SEM. Asterisks in (C) indicate significant differences between days. * $p < 0.05$, ** $p < 0.01$.*

DISCUSSION

We investigated and systematically compared the intra- and post-anesthetic effects of different commonly used anesthetic strategies on the mouse hippocampus across multiple levels of analysis. Despite sharing some common traits, brain and cellular network states differ substantially under the influence of various types of anesthetics (Clark and Rosner, 1973; Sarasso et al., 2015; Steriade et al., 1993). Indeed, at the neuronal level, compared with awake state, all three anesthetics showed robustly reduced spiking activity in single neurons, reduced power in high oscillation frequency band, and decorrelated cellular population activity.

bioRxiv preprint doi: https://doi.org/10.1101/2020.06.05.135905; this version posted June 6, 2020. The copyright holder for this preprint (which was not certified by peer review) is the author/funder. All rights reserved. No reuse allowed without permission.

However, the induced network states in CA1 were highly distinct between the three different conditions, with Iso leading to prominent network oscillations at around 0.1 Hz, which timed the spiking activity of single units and neuronal calcium transients. Keta/Xyl caused pronounced oscillations between 0.5 and 4 Hz and the strongest reduction in calcium dynamics. MMF, in contrast, most strongly reduced LFP and SUA and impaired population dynamics as assessed with calcium imaging. Differences were also present in the long-term effects on spine dynamics, with Keta/Xyl stabilizing spines, leading to reduced turnover and increased density. MMF, on the other hand, mildly increased spine dynamics. Keta/Xyl cannot be antagonized and therefore changes of the CA1 network mediated by this anesthetic strategy had the longest duration, in agreement with long-lasting overall changes of global animal physiology (Albrecht et al., 2014). More unexpectedly, and in contrast to overall effects on physiology (Albrecht et al., 2014), CA1 network dynamics were still disturbed long after antagonization of MMF anesthesia. These long-lasting alterations were associated with impairment of episodic memory consolidation after exposure to Keta/Xyl- or MMF, but not Iso. Thus, despite fulfilling all the hallmarks of general anesthesia, different GAs distinctly alter hippocampal network dynamics, synaptic connectivity, and memory consolidation.

Iso, MMF and Keta/Xyl have different molecular targets and distinctly modulate functional and structural features of CA1

The GAs used here represent three different strategies based on the large repertoire of currently available anesthetics. Isoflurane represents the class of halogenated diethyl ether analogues, which are volatile and therefore administered via inhalation. Fentanyl, in combination with the analgesic medetomidine and the sedative midazolam (MMF), represents an anesthetic approach based on injection of a combination of drugs with sedative, analgesic and anxiolytic properties. In the clinic, propofol can be used instead of midazolam. Finally, ketamine is used both as an anesthetic and, at lower dosage, as a treatment against depression. For anesthesia it is combined with xylazine, which acts sedative, analgesic and as a muscle relaxant. All three strategies differ markedly in their molecular targets. Consequently, they uniquely modulate general animal physiology (Albrecht et al., 2014) and brain activity (Sarasso et al., 2015). Isoflurane is a potent GABA- and glycine receptor agonist. Moreover, it activates two-pore potassium channels and acts as α-amino-3-hydroxy-5-methyl-4-isoxazolepropionic acid receptor (AMPAR) inhibitor (Alkire et al., 2008). Similar to Iso, midazolam, the hypnotic component of the MMF mix, mainly acts as a GABAR agonist with little effect on NMDARs. In contrast, ketamine is a potent, use-dependent NMDAR blocker with less pronounced effects on potassium channels, GABA, glycine and other glutamate receptors such AMPA or kainite receptors (Alkire et al., 2008). Moreover, while most anesthetics reduce activity of thalamic nuclei, ketamine increases thalamic drive (Langsjo et al., 2005), leading to enhanced rather than reduced oscillations in mid-to-high frequency bands such as theta and gamma (Lee et al., 2013; Soltesz and Deschenes, 1993). In accordance with this, our study reveals major differences in the action of the different anesthetics on functional and structural features of CA1. With both electrical recordings and calcium imaging we report a robust reduction of neuronal spiking and pairwise neuronal correlation. Notably, effects on electrical activity and calcium activity were well in line for both Iso and MMF, despite the different recording methods. However, we observed some divergence for Keta/Xyl.

Comparison of electrophysiological recordings and calcium imaging

Generally, differences in electrophysiological recordings and calcium imaging data may stem from the location where the signal is detected. In the calcium imaging experiments, the signal

bioRxiv preprint doi: https://doi.org/10.1101/2020.06.05.135905; this version posted June 6, 2020. The copyright holder for this preprint (which was not certified by peer review) is the author/funder. All rights reserved. No reuse allowed without permission.

was sampled in a horizontal plane located inside and parallel to stratum pyramidale of CA1. In this configuration, somatic, action-potential driven calcium transients mainly from pyramidal neurons dominate the signal. Due to the kinetics and calcium-binding properties of GCaMP6f, action potentials can only be resolved below approx. 5 Hz and are reported non-linearly (Chen et al., 2013). In contrast, the electrodes on linear probes are arranged orthogonally to the strata of CA1 and parallel to the dendrites of CA1 cells. Thus, synaptic potentials mainly constitute the LFP across all layers and spikes are picked up from both pyramidal cells (in stratum pyramidale) and GABAergic neurons in all layers. Moreover, the first method samples neurons that spatially distribute over a large area. In contrast, the second one is biased towards large, active neurons that are in close proximity of the electrode.

More specifically, under Keta/Xyl, the overall firing rate of single units showed the smallest reduction of all three anesthetics. At the same time, imaging revealed the most substantial reduction in rate, amplitude and duration of calcium transients (compare Fig. 2B and 3D). One reason for this discrepancy may be the inhibitory action of ketamine on NMDARs. CA1 pyramidal cells display large, NMDAR-driven dendritic plateau potentials and calcium spikes (Katz et al., 2009). Moreover, ketamine likely inhibits L-type voltage-gated calcium channels (Yamakage et al., 1995) and reduces burst firing (Yang et al., 2018), leading to calcium transients with reduced amplitude and a faster decay constant. In contrast, ketamine has little influence on sodium spikes and AMPAR-mediated synaptic potentials, which are detected in electrical recordings as SUA and LFP, respectively. In accordance with electrical recordings, calcium transients showed increased power at 0.1-0.2 Hz under Iso. However, we did not detect a clear peak at 1-4 Hz in the presence of Keta/Xyl, as seen in LFP and SUA, probably due to its strongly dampening effect on calcium transients. The (low-pass) filtering of neuronal activity imposed by calcium indicators might also play a role.

Notably, the differences between electrical recordings and calcium imaging under Keta/Xyl are relevant. Calcium is a second messenger central to neuronal plasticity and metabolism (West et al., 2002; Wiegert and Bading, 2011). NMDARs are a major source for activity-dependent calcium entry into the cell, involved in regulating synaptic plasticity, metabolism, and pathology (Hardingham and Bading, 2010). The present findings suggest that Keta/Xyl has a particularly strong effect on neuronal calcium activity, uncoupling action potential firing from associated cytosolic calcium transients, leading to reduced intracellular calcium signaling. In contrast, calcium transients under MMF and Iso anesthesia closely matched the electrical activity profile of neurons. Therefore, aside from overall effects on network activity, Keta/Xyl may selectively alter neuronal plasticity by suppressing NMDAR-dependent postsynaptic calcium signals.

In contrast to neocortex, GAs decorrelate neuronal activity in CA1

All anesthetics decorrelated neuronal activity in CA1, leading to an overall more fragmented network state. This is in stark contrast with what has been reported from studies on GAs and cortical activity both at adulthood (Goltstein et al., 2015; Greenberg et al., 2008; Wenzel et al., 2019) and during development (Chini et al., 2019). This discrepancy may arise from the distinct architecture of CA1 compared to L2/3 of the neocortex, the latter showing a high degree of local interconnectivity (Harris and Mrsic-Flogel, 2013). In CA1 this is not the case. Pyramidal cells receive their main excitatory input from CA3 and entorhinal cortex and send their efferents to subiculum and extrahippocampal areas without making local connections among each other (Neves et al., 2008). Afferent activity originating in various sources and converging in CA1, may arrive out-of-phase under anesthesia, leading to desynchronized firing of CA1 pyramidal cells. Such a phenomenon has been proposed as a candidate mechanism underlying

bioRxiv preprint doi: https://doi.org/10.1101/2020.06.05.135905; this version posted June 6, 2020. The copyright holder for this preprint (which was not certified by peer review) is the author/funder. All rights reserved. No reuse allowed without permission.

desynchronization of neuronal firing in basal ganglia under conditions of slow oscillations (slow-wave sleep) and high synchrony in the neocortex (Mizrahi-Kliger et al., 2018). Notably, pairwise correlation was not entirely independent of the distance between neurons. Synchronization of pyramidal neurons via local, GABAergic interneurons may be another factor that increases spatial correlations. Both in neocortex and hippocampus, various types of GABAergic interneurons locally connect to and synchronize pyramidal neurons such as basket or bistratified cells (Klausberger and Somogyi, 2008).

Coordinated neuronal network dynamics, including pairwise correlation of calcium transients and single units, population coupling, clustering in the temporal and spatial domain were consistently impaired most strongly with Keta/Xyl and MMF. Iso, both in electrophysiological as well as calcium recordings, showed the mildest effects and permitted hippocampal activity patterns that closely resembled the awake state. Iso and MMF, in contrast to Keta/Xyl, are thought to be immediately reversible (Albrecht et al., 2014). However, they showed significant disruption of network dynamics for at least 45 min after reversal. Thus, all anesthetics had a much longer effect on network activity than expected. We therefore further asked whether this is reflected in long-term effects of these different types of anesthetics on spine dynamics of CA1 pyramidal neurons. Recent studies investigating spine dynamics at CA1 pyramidal neurons came to incongruent conclusions reporting spine turnover ranging from 3% (Gu et al., 2014) over 12% (Attardo et al., 2015) to approx. 80% (Pfeiffer et al., 2018) over 4 days. However, all studies used either isoflurane (Attardo et al., 2015) or ketamine/xylazine-based (Gu et al., 2014; Pfeiffer et al., 2018) anesthesia during the repeated imaging sessions. Thus, to what extent anesthesia itself influences spine dynamics is not clear.

Iso, MMF and Keta/Xyl distinctly alter spine dynamics in CA1

More generally, various effects of general anesthesia on spine dynamics were reported, depending on the brain region, preparation, age of the animal and anesthetic strategy. For example, enhanced synaptogenesis has been reported with different types of anesthetics on cortical and hippocampal neurons during development (Briner et al., 2010; De Roo et al., 2009). In contrast, one study indicated that spine dynamics were not altered on cortical neurons of adult mice with Keta/Xyl or Iso (Yang et al., 2011), while another study demonstrated an increase in spine density in somatosensory cortex with ketamine (Pryazhnikov et al., 2018). Also, fentanyl-mediated, concentration-dependent bidirectional modulations of spine dynamics were reported in hippocampal cultures (Lin et al., 2009).

To systematically compare spine dynamics in CA1 in vivo under different anesthetic treatments, we imaged spines at basal, oblique and tuft dendrites in a large set of dendrites. We found small, but robust chronic effects of repeated anesthesia. Keta/Xyl decreased spine turnover leading to a mild increase in spine density over time by stabilizing existing spines. This observation agrees with recent studies that showed a stabilizing effect of ketamine in the somatosensory cortex, resulting in increased spine density (Pryazhnikov et al., 2018). Thus, repeated anesthetic doses of Keta/Xyl may limit overall synaptic plasticity and thus, spine turnover. It was further shown that sub-anesthetic, antidepressant doses of ketamine enhance spine density in the prefrontal cortex (Li et al., 2010; Phoumthipphavong et al., 2016), similar to our study for CA1 neurons. Iso and MMF had contrasting effects on spine dynamics compared to Keta/Xyl, mildly enhancing spine turnover, which might be explained by, the their different pharmacology compared to ketamine, as pointed out above. A second aspect that distinguishes Keta/Xyl from Iso and MMF is its irreversibility, which might lead to longer-lasting alterations of synaptic transmission and E/I ratios leading to differential spine dynamics. This

bioRxiv preprint doi: https://doi.org/10.1101/2020.06.05.135905; this version posted June 6, 2020. The copyright holder for this preprint (which was not certified by peer review) is the author/funder. All rights reserved. No reuse allowed without permission.

idea is supported by the observation that during the anesthesia period itself, spine turnover was not altered, suggesting that long-lasting and repeated disturbances are required to leave a mark in synaptic connectivity.

MMF and Keta/Xyl, but not Iso, retrogradely affect episodic-like memory formation

Notably, a single dose of anesthesia with Keta/Xyl and MMF, but not Iso disrupted memory consolidation using a water maze assay in adult mice. Our results appear at odds with a reports (Zurek et al., 2012), where a single, 1-h treatment with Iso caused deficits in the formation of contextual fear memory, object recognition memory and in the Morris water maze in the following 48 h. However, this study investigated memory acquisition after anesthesia (i.e. anterograde amnesia), while our study asked whether anesthesia affects the consolidation of a memory formed shortly before the treatment (i.e. retrograde amnesia). The induction of retrograde amnesia correlated with the magnitude and duration of CA1 network disturbance imposed by the various anesthetics. KetaXyl and MMF most strongly decorrelated CA1 network activity and these disruptions recovered only slowly, compared to Iso.

Changes in synaptic connections are considered essential for memory formation and storage (Frey and Morris, 1997; Kasai et al., 2010; Segal, 2005; Yang et al., 2009). Despite, a small effect on spine dynamics, the strong and lasting disturbance of hippocampal network activity in CA1 (and most likely other brain areas) by Keta/Xyl and MMF was sufficient to interfere with memory consolidation. The chronic alterations of spine turnover, especially by Keta/Xyl, may therefore indicate that repeated anesthesia can impact long-lasting hippocampus-dependent memories. To establish a direct link between spine dynamics, network disruptions and memory, future studies are required that investigate both spine turnover and changes in population coupling at hippocampal neurons causally involved in memory formation and maintenance.

Taken together, we report a novel effect of anesthesia on brain dynamics, namely fragmentation of network activity in hippocampus. We consistently observe this phenomenon across multiple levels of analysis. This unique response compared to the cortex may underlie its high sensitivity to anesthesia including its central role in amnesia. The extent, duration, and reversibility of network fragmentation depends on the GA used. Therefore, this study may help guide the choice of an appropriate anesthetic strategy, dependent on experimental requirements and constraints, especially in the neurosciences. More generally, our findings might also have relevance for the clinic. Postoperative delirium, a condition that involves memory loss, is still an unresolved mystery. Minimizing the disturbance of hippocampal function may be one building block to overcome this undesired condition.

bioRxiv preprint doi: https://doi.org/10.1101/2020.06.05.135905; this version posted June 6, 2020. The copyright holder for this preprint (which was not certified by peer review) is the author/funder. All rights reserved. No reuse allowed without permission.

AUTHOR CONTRIBUTIONS

Conceptualization, W.Y., M.C., J.S.W.; Methodology, W.Y., M.C., J.A.P., A.F., F.M., O.S., I.L.H.-O., J.S.W.; Analysis, W.Y., M.C., A.F., J.A.P., P.P., C.R., F.M., J.S.W.; Investigation , W.Y., J.A.P.; Data Curation, W.Y., M.C., J.A.P., A.F.; Writing, W.Y., M.C., O.S., I.L.H.-O., J.S.W.; Visualization, W.Y., M.C., A.F., J.S.W.; Supervision, F.M., I.L.H.-O., J.S.W.; Project Administration, J.S.W.; Funding Acquisition, W.Y., A.F., I.L.H.-O., J.S.W.

ACKNOWLEDGEMENTS

We thank Stefan Schillemeit and Kathrin Sauter for technical assistance and Thomas G. Oertner and Amit Marmelstein for critical feedback on the manuscript. This work was funded by the Deutsche Forschungsgemeinschaft (DFG, SPP1926/FOR2419/P6, SFB963/B8 to J.S.W., SPP 1665/Ha 4466/10-1/Ha4466/12-1, SFB 936/B5 to I.L.H.-O.), the European Research Council (ERC2016-StG-714762 to J.S.W., ERC-2015-CoG 681577 to I.L.H.-O.), the German Academic Exchange Service (DAAD, STG/19/5744091 to A.F.), and the Chinese Scholarship Council (CSC 201606210129 to W.Y.).

DECLARATION OF INTERESTS

The authors declare no competing interests.

STAR METHODS

Key Resources Table

Resource Availability

Lead Contact

Further information and requests for resources and reagents should be directed to and will be fulfilled by the Lead Contact, J. Simon Wiegert (simon.wiegert@zmnh.uni-hamburg.de).

Materials Availability

This study did not generate new unique reagents.

Data and Code Availability

The code generated during this study is available at https://github.com/OpatzLab/HanganuOpatzToolbox and https://github.com/mchini/Calcium-Imaging---Anesthesia

The calcium imaging and electrophysiology data sets generated during this study are available at https://gin.g-node.org/SW_lab/Anesthesia_CA1

Experimental Model and Subject Details

Mice

Adult C57BL/6J mice and transgenic Thy1-GFP-M mice of both sexes were housed and bred in pathogen-free conditions at the University Medical Center Hamburg-Eppendorf. The light/dark cycle was 12/12 h and the humidity and temperature were kept constant (40% relative humidity; 22°C). Food and water were available ad libitum. All procedures were performed in compliance with German law according and the guidelines of Directive 2010/63/EU. Protocols were approved by the Behörde für Gesundheit und Verbraucherschutz of the City of Hamburg.

bioRxiv preprint doi: https://doi.org/10.1101/2020.06.05.135905; this version posted June 6, 2020. The copyright holder for this preprint (which was not certified by peer review) is the author/funder. All rights reserved. No reuse allowed without permission.

Method Details

Hippocampal recording-window surgery and in-vivo electrophysiology

Chronic multisite extracellular recordings were performed in dorsal CA1. The adapter for head fixation was implanted at least 4 days before recordings. Mice were anesthetized via intraperitoneal injection of midazolam/medetomidine/fentanyl (MMF) and placed on a heating blanket to maintain the body temperature. Eyes were covered with eye ointment (Vidisic, Bausch + Lomb) to prevent drying. Prior to surgery, the depth of anesthesia and analgesia was evaluated with a toe-pinch to test the paw-withdrawal reflex. Subsequently, mice were fixed in a stereotactic frame, the fur was removed with a fine trimmer and the skin of the head was disinfected with Betaisodona. After removing the skin, 0.5% bupivacaine / 1% lidocaine was locally applied to cutting edges. A metal head-post (Neurotar) was attached to the skull with dental cement (Super Bond C&B, Sun Medical) and a craniotomy was performed above the to the dorsal CA1 area (− 2.0 mm AP, ± 1.3 mm ML relative to Bregma) which was subsequently protected by a customized synthetic window filled with Kwik-Cast sealant (World Precision Instruments). After recovery from anesthesia, mice were returned to their home cage and were provided with Meloxicam mixed into soft food for 3 days. After recovery from the surgery, mice were accustomed to head-fixation and trained to move in the Mobile HomeCage system (Neurotar). For recordings, craniotomies were reopened by removal of the Kwik-Cast sealant and multi-site electrodes (NeuroNexus, MI, USA) were inserted into the dorsal CA1 (one-shank, A1x16 recording sites, 50 µm spacing, 1.6 mm deep). A silver wire served as ground and reference in the craniotomy between skull and brain tissue. Extracellular signals were band-pass filtered (0.1-8000 Hz) and digitized (32 kHz) with a multichannel extracellular amplifier (Digital Lynx SX; Neuralynx). The same animals were recorded weekly under different anesthesia. After 15 min of non-anesthetized recording, mice received a subcutaneous injection of Keta/Xyl, MMF or inhalation of Iso in a pseudo-randomized order. The following drug combinations were administered: 2.0 % isoflurane in 100% O_2; 130 mg/kg ketamine, 10 mg/kg xylazine s.c.; 5.0 mg/kg midazolam, 0.2 mg/kg medetomidine and 0.05 mg/kg fentanyl s.c.; and for complete reversal of anesthesia, 0.5 mg/kg flumazenil, 2.5 mg/kg atipamezole and 0.1 mg/kg buprenorphine s.c. Recordings were continued for 1.5 h. After recordings craniotomy was closed and mice were returned to their home cage. Electrode position was confirmed in brain slices postmortem.

Virus injection and hippocampal window surgery for in vivo calcium imaging

C57BL/6J wild-type mice were anesthetized via intraperitoneal injection of midazolam/medetomidine/fentanyl (MMF) and placed on a heating blanket to maintain the body temperature. Eyes were covered with eye ointment (Vidisic, Bausch + Lomb) to prevent drying. Prior to surgery, the depth of anesthesia and analgesia was evaluated with a toe-pinch to test the paw-withdrawal reflex. Subsequently, mice were fixed in a stereotactic frame, the fur was removed with a fine trimmer and the skin of the head was disinfected with Betaisodona. The skin was removed by a midline scalp incision (1-3 cm), the skull was cleaned using a bone scraper (Fine Science Tools) and a small hole was drilled with a dental drill (Foredom) above the injection site. AAV2/7-syn-GCaMP6f was targeted unilaterally to the dorsal CA1 area (− 2.0 mm AP, ± 1.3 mm ML, − 1.5 mm DV relative to Bregma). 0.6 µl of virus suspension was injected. All injections were done at 100 nl*min^{-1} using a glass micropipette. After the injection, the pipette stayed in place for at least 5 min before it was withdrawn and the scalp was closed with sutures. For complete reversal of anesthesia, mice received a subcutaneous dose of Flumazenil, Atipamezol and Buprenorphine (FAB). During the two days following surgery animals were provided with Meloxicam mixed into soft food. Two weeks after virus injection,

bioRxiv preprint doi: https://doi.org/10.1101/2020.06.05.135905; this version posted June 6, 2020. The copyright holder for this preprint (which was not certified by peer review) is the author/funder. All rights reserved. No reuse allowed without permission.

mice were anesthetized as described above to implant the hippocampal window. After fur removal, skin above the frontal and parietal bones of the skull was removed by one horizontal cut along basis of skull and two rostral cuts. The skull was cleaned after removal of the periosteum, roughened with a bone scraper and covered with a thin layer of cyanoacrylate glue (Pattex). After polymerization a 3-mm circle was marked on the right parietal bone (anteroposterior, −2.2 mm; mediolateral, +1.8 mm relative to bregma) with a biopsy punch and the bone was removed with a dental drill (Foredom). The dura and somatosensory cortex above the hippocampus were carefully aspirated until the white matter tracts of the corpus callosum became visible. The craniotomy was washed with sterile PBS and a custom-built imaging window was inserted over the dorsal hippocampus. The window consisted of a hollow glass cylinder (diameter: 3 mm, wall thickness: 0.1 mm, height: 1.8 mm) glued to a No. 1 coverslip (diameter: 3mm, thickness: 0.17 mm) on the bottom and to a stainless-steel rim on the top with UV-curable glass glue (Norland NOA61). The steel rim and a head holder plate (Luigs & Neumann) were fixed to the skull with cyanoacrylate gel (Pattex). After polymerization, cranial window and head holder plate were covered with dental cement (Super Bond C&B, Sun Medical) to provide strong bonding to the skull bone. Following the surgery, animals were provided with Meloxicam mixed into soft food for 3 days. The position of the hippocampal window was confirmed in brain slices postmortem.

Two-photon calcium imaging in anesthetized and awake mice

The same animals were sequentially imaged under Keta/Xyl, MMF or Iso in a pseudo-randomized order (for details see above). After losing the righting reflex, generally 5–10 min after application of the anesthetics, the animals were positioned on a heating-pad to maintain body temperature at approximately 37°C during anesthesia. The intensity of anesthesia and evaluation of the different stages of anesthesia were assessed by recording the presence or absence of distinct reflex responses: righting reflex, palpebral reflex, toe-pinch reflex. Between each imaging session, mice were allowed to recover for one week.

Anesthetized mice were head fixed under the microscope on a heated blanket to maintain body temperature. Eyes were covered with eye ointment (Vidisic, Bausch + Lomb) to prevent drying. The window was centered under the two-photon microscope (MOM-scope, Sutter Instruments, modified by Rapp Optoelectronics) and GCaMP6f expression was verified in the hippocampus using epi fluorescence. Images were acquired with a 16x water immersion objective (Nikon CFI75 LWD 16X W, 0.80 NA, 3.0 mm WD). For awake imaging we used a linear treadmill, which allowed imaging during quiet and running states. 5-min-timelapse images were acquired every 10 minutes for a period of 50 minutes. Image acquisition was carried out with a Ti:Sa laser (Chameleon Vision-S, Coherent) tuned to 980 nm to excite GCaMP6f. Single planes (512x512 pixels) were acquired at 30 Hz with a resonant-galvanometric scanner at 29-60 mW (980 nm) using ScanImage 2017b (Vidrio). Emitted photons were detected by a pair of photomultiplier tubes (H7422P-40, Hamamatsu). A 560 DXCR dichroic mirror and 525/50 and 607/70 emission filters (Chroma Technology) were used to separate green and red fluorescence. Excitation light was blocked by short-pass filters (ET700SP-2P, Chroma). For the repetitive imaging, the position of the field of view (FOV) was registered in the first imaging session with the help of vascular landmarks and cell bodies of CA1 pyramidal neurons. This allowed for subsequent retrieval of the FOV for each mouse.

Two-photon spine imaging in anesthetized and awake mice

3 - 4 weeks after window implantation, chronic spine imaging started in Tg(Thy1-EGFP)MJrs/J mice with the first of a total of four imaging series (see Fig. S11A). Each imaging series was

bioRxiv preprint doi: https://doi.org/10.1101/2020.06.05.135905; this version posted June 6, 2020. The copyright holder for this preprint (which was not certified by peer review) is the author/funder. All rights reserved. No reuse allowed without permission.

done under one of the three anesthetic conditions (Iso, Keta/Xyl, MMF, see above for details) or during wakefulness. Within one series, mice were imaged 5 times every 4 days. Afterwards, mice were allowed to recover for three to four weeks until the next imaging series under a different anesthetic condition was started. Thus, each experiment lasted approx. 5 months. To avoid time-dependent effects, anesthetic conditions were pseudo-randomized (see Fig. S11A). For imaging sessions under anesthesia mice were head fixed under the microscope on a heated blanket to maintain body temperature. Eyes were covered with eye ointment (Vidisic, Bausch + Lomb) to prevent drying. The window was centered under the two-photon microscope (MOM-scope, Sutter Instruments, modified by Rapp Optoelectronics) and GFP expression was verified in the hippocampus using epi-fluorescence. Image acquisition was carried out with a Ti:Sa laser (Chameleon Vision-S, Coherent) tuned to 980 nm to excite GFP. Images were acquired with a 40x water immersion objective (Nikon CFI APO NIR 40X W, 0.80 NA, 3.5 mm WD). Single planes (512x512 pixels) were acquired at 30 Hz with a resonant scanner at 10-60 mW (980 nm) using ScanImage 2017b. Before the first imaging session, we registered the field of views with the help of vascular landmarks and cell bodies of CA1 pyramidal neurons and selected several regions for longitudinal monitoring across the duration of the time-lapse experiment. Each of these regions contained between 1 and 2 dendritic segments visibly expressing GFP. The imaging sessions lasted for max 60 min and mice were placed back to their home cages where they woke up.

Morris Water Maze

We designed a protocol for reversal learning in the spatial version of the water maze to assess the possible effects of the different anesthetics on episodic-like memory in mice (Chen et al., 2000; Morellini, 2013). The water maze consisted of a circular tank (145 cm in diameter) circled by dark curtains and walls. The water was made opaque by the addition of non-toxic white paint such that the white platform (14 cm diameter, 9 cm high, 1 cm below the water surface) was not visible. Four landmarks (35 X 35 cm) differing in shape and grey gradient were positioned on the wall of the maze. Four white spotlights on the floor around the swimming pool provided homogeneous indirect illumination of 60 lux on the water surface. Mice were first familiarized for one day to swim and climb onto a platform (diameter of 10 cm) placed in a small rectangular maze (42.5 x 26.5 cm and 15.5 cm high). During familiarization, the position of the platform was unpredictable since its location was randomized, and training was performed in darkness. After familiarization, mice underwent three learning days, during which they had to learn the location of a hidden platform. The starting position and the side of the maze from which mice were taken out of the maze were randomized. At day 1 mice underwent four learning trials (maximum duration of 90 seconds, inter-trial interval of 10 minutes). After staying on the platform for 15 s, mice were returned to their home cage and warmed up under red light. On day 2, mice underwent two training trials before they performed a 60 seconds-long probe trial to assess their searching strategy. Afterwards, one additional training trial was used to re-consolidate the memory of the platform position. On day 3 the long-term memory of the platform position was tested with a 45-seconds long probe trial, followed by another training trial with the platform in place to avoid extinction. Then mice underwent four reversal learning trials with the platform located in the quadrant opposite to the one in which the platform was during the previous training trials. To assess whether the mice learned the new platform position, mice underwent a 60-seconds long probe trial to followed by one more training trial to consolidate the memory of the new location. One hour after the last reversal learning trial, mice were anesthetized to analyze the effects of the anesthesia on the consolidation of the memory of the new platform position. Mice were assigned to four groups with an equal average performance during the probe trial on day 2. Each group was subjected to different conditions:

bioRxiv preprint doi: https://doi.org/10.1101/2020.06.05.135905; this version posted June 6, 2020. The copyright holder for this preprint (which was not certified by peer review) is the author/funder. All rights reserved. No reuse allowed without permission.

one-hour Iso anesthesia, one-hour MMF anesthesia, Keta/Xyl anesthesia (which was not antagonized), and one group was left untreated. On day 4, mice underwent a 60-seconds long probe trial to evaluate their searching strategies, namely, the "episodic-like memory" of the reversal learning trials performed one hour before having been anesthetized on day 3 (see Fig. 8A).

Quantification and Statistical Analysis

Electrophysiology

In vivo electrophysiology data were analyzed with custom-written scripts in the Matlab environment available at https://github.com/mchini/HanganuOpatzToolbox. Data were band-pass filtered (1-100 Hz or 0-100 Hz for low frequency LFP analysis) using a third-order Butterworth forward and backward filter to preserve phase information before down-sampling to analyze LFP.

Detection of active periods. Active periods were detected with an adapted version of an algorithm for ripple detection (https://github.com/buzsakilab/buzcode/blob/master/detectors/detectEvents/bz_FindRipples.m). Briefly, active periods were detected on the band-pass filtered (4-20 Hz) normalized squared signal using both absolute and relative thresholds. We first passed the signal through a boxcar filter and then performed hysteresis thresholding: we first detected events whose absolute or relative power exceeded the higher threshold, and considered as belonging to the same event all data points that were below the lower (absolute or relative) threshold. Absolute thresholds were set to 7 and 15 µV, relative thresholds to 1 and 2. Periods were merged if having an inter-period interval shorter than 900 ms, and discarded if lasted less than 500 ms. Percentage of active periods was calculated for 15 min bins. Timestamps were preserved for further analysis.

Power spectral density. Power spectral density was calculated on 30 s-long windows of 0-100 Hz filtered signal using Welch's method with a signal overlap of 15 s.

Modulation index (MI). Modulation index was calculated as (value anesthesia - value pre-anesthetized) / (value anesthesia + value pre-anesthetized).

Power law decay exponent of the LFP power spectrum. The 1/f slope was computed as in (Gao et al., 2017). We used robust linear regression (Matlab function *robustfit.m*) on the log10 of the LFP power spectrum in the 30-50 Hz frequency range.

Phase-amplitude coupling (PAC). PAC was calculated on 0-100 Hz filtered full signal using the PAC toolbox based on modulation index measure (Onslow et al., 2011). Range of phase vector was set to 0-8 Hz and range of amplitude vector was set to 20-100 Hz. Significant coupling was calculated in comparison to a shuffled dataset. Non-significant values were rejected.

Single unit analysis. Single unit activity (SUA) was detected and clustered using klusta (Rossant et al., 2016) and manually curated using phy (https://github.com/cortex-lab).

Active units: the recording was divided into 15-minute bins. Single units were considered to be active in the time interval if they fired at least five times.

Pairwise phase consistency. Pairwise phase consistency (PPC) was computed as previously described (Vinck et al., 2010). Briefly, the phase in the band of interest was extracted as mentioned above, and the mean of the cosine of the absolute angular distance (dot product) among all single unit pairs of phases was calculated.

bioRxiv preprint doi: https://doi.org/10.1101/2020.06.05.135905; this version posted June 6, 2020. The copyright holder for this preprint (which was not certified by peer review) is the author/funder. All rights reserved. No reuse allowed without permission.

Unit Power. SUA spike trains of each recording were summed in a population vector, and power spectral density was calculated on 30 s-long windows using Welch's method with a signal overlap of 15 s. The resulting power spectra were normalized by the firing rate in that window.

Spike-Time tiling coefficient (STTC) was computed as previously described (Cutts and Eglen, 2014). Briefly, we quantified the proportion (P_A) of spikes of spike train A that fall within ±Δt of a spike from spike train B. To this value we subtract the proportion of time that occurs within ±Δt of spikes from spike train B (T_B). This is then divided by 1 minus the product of these two values. The same is then applied after inverting spike train A and B, and the mean between the two values is kept.

$$STTC = \frac{1}{2}\left(\frac{P_A - T_B}{1 - P_A T_B} + \frac{P_B - T_A}{1 - P_B T_A}\right)$$

Importantly, this coefficient has several desirable properties. It is bounded between -1 and 1. It is symmetric with respect to the two spike trains. Computing it over different timescales is readily done by controlling the value of the parameter "Δt". Lastly, and most importantly, traditionally used methods of assessing correlations between pairs of spike trains show an inverse correlation between their value and firing rate, due to the fact that spiking is sparse with respect to the sampling frequency, and therefore quiescent period in both spike trains artificially increase the correlation. This is not the case for the spike-time tiling coefficient (Cutts and Eglen, 2014). Given that there are large differences in the average firing rate of our conditions, we chose STTC analysis over pure correlation analysis to circumvent this major bias. On the flipside, STTC cannot be straightforwardly applied to negative correlations, that were therefore not investigated in SUA data.

<u>*Calcium imaging data*</u>

In vivo calcium imaging data were analyzed with custom-written scripts in the Python and Matlab environment available at https://github.com/mchini/Calcium-Imaging---Anesthesia.

Alignment of multiple recordings. To track the activity of the same set of neurons in different anesthetic conditions and during wakefulness, we acquired two-photon time series of a defined field of view for each animal and each condition across multiple weeks. Over such long time periods, the field of view was susceptible to geometrical transformations from one recording to another and thus, any two time series were never perfectly aligned. This problem scaled with time that passed between recordings. However, optimal image alignment is critical for the successful identification and calcium analysis of the same neurons across time (Rose et al., 2016; Sheintuch et al., 2017).

To address this problem, we developed an approach based on the pystackreg package, a Python implementation of the ImageJ extension TurboReg/StackReg (Thevenaz et al., 1998). The source code that reproduces the procedure described in this section is available on github (https://pypi.org/project/pystackreg/). The *pystackreg* package is capable of using different combinations of geometrical transformations for the alignment. We considered rigid body (translation + rotation + scaling) and affine (translation + rotation + scaling + shearing) transformation methods, which we applied to mean and enhanced-mean intensity images generated by Suite2p during the registration of each single recording. We performed the alignment using all four combinations (2 transformations x 2 types of images) choosing the one with the best performance according to the following procedure. Squared difference between the central part of a reference and aligned image served as a distance function d to quantify

bioRxiv preprint doi: https://doi.org/10.1101/2020.06.05.135905; this version posted June 6, 2020. The copyright holder for this preprint (which was not certified by peer review) is the author/funder. All rights reserved. No reuse allowed without permission.

the alignment (since the signal is not always present on the borders of the image they were truncated):

$$d = \sum_{i,j}^{\substack{Tranc.\\images}} (x_{i,j}^{ref} - x_{i,j}^{aligned})^2,$$

where $x_{i,j}^{ref}$ and $x_{i,j}^{aligned}$ are intensities of the pixel with coordinates i, j of the reference and aligned images. The combination with the smallest score was chosen for the final transformation. In some rare cases, the algorithm of the alignment did not converge for a given transformation method and image type (mean or enhanced-mean), crumbling the aligned image in a way that most of the field of view remained empty. This combination may have the smallest distance function *d* and may be falsely identified as the best one. To overcome this issue, an additional criterion was applied, which requires the central part of the aligned picture to contain more than 90 % of the non-empty pixels. The overall performance of the algorithm was verified by visual inspection. An example of the alignment of two recordings is shown in Fig. S5. The alignment for all recordings of an example mouse is demonstrated in a supplementary video (Supplementary_video_37529_aligned_recordings.avi).

In case of relatively small distortions across recordings, for example, when consecutive acquisitions were done within one imaging session, registration can alternatively be performed simultaneously with ROI detection in Suite2p by concatenating those TIFF-stacks. In this approach, every ROI is automatically labeled with the same identification number across all recordings.

Identification of the same neurons across different recordings & unique neuron ID assignment. After the alignment procedure, we set out to identify neurons which were active across multiple recordings (and thus, multiple conditions). To achieve this, we developed an algorithm similar to the one described in Sheintuch. et al. 2017 (Sheintuch et al., 2017)

The algorithm processes in series all recordings for a given animal and assigns unique identification (ID) numbers to each ROIs of every recording. Since the recordings under Iso-anesthesia had the largest number of active neurons, we chose the first recording of this condition as reference. We assigned IDs that ranged from 1 to the total amount of neurons to all the ROIs of this recording. For every other recording of each mouse, Neuron ID assignment consisted of: 1. comparison of the properties (details below) of each ROI with each ROI that had already been processed. 2a. If the properties of the ROI matched the properties of an ROI from a previously analyzed recording, the ROI received the same Neuron ID. 2b. If no match was found, a new (in sequential order) Neuron ID was assigned to the ROI. In order to be identified as representing the same neuron in two different recordings, two ROIs had to respect the following criteria: the distance between their centroids had to be below 3 µm, and the overlap between their pixels had to be above 70%. An example of the identification of unique neuron pairs in two recordings is presented in Fig. S6A. The thresholds were chosen based on the distribution of the distances between centroids and percentage of the overlaps. An example for a single mouse is graphically illustrated in Fig. S6B. Both properties have a clearly bimodal distribution (similar to (Sheintuch et al., 2017)) with cutoffs close to the chosen thresholds.

Signal extraction and analysis. Signal extraction, correlation and spectral analysis for calcium signal was performed using Python (Python Software Foundation, NH, USA) in the Spyder (Pierre Raybaut, The Spyder Development Team) development environment. Calcium imaging

bioRxiv preprint doi: https://doi.org/10.1101/2020.06.05.135905; this version posted June 6, 2020. The copyright holder for this preprint (which was not certified by peer review) is the author/funder. All rights reserved. No reuse allowed without permission.

data were analyzed with the Suite2p toolbox (Pachitariu et al., 2017) using the parameters given in table 1.

Parameter	**Variable**	**Value**
Sampling rate, frames per second	fs	30
Registration		
Subsampled frames for finding reference image	nimg_init	2000
Number of frames per batch	batch_size	200
Maximum allowed registration shift, as a fraction of frame max(width and height)	maxregshift	0.1
Precision of subpixel registration (1/subpixel steps)	subpixel	10
Smoothing	smooth_sigma	1.15
Bad frames to be excluded	th_badframes	100.0
Non-rigid registration		
Use nonrigid registration	nonrigid	True
Block size to register (** keep this a multiple of 2 **)	block_size	[128,128]
if any nonrigid block is below this threshold, it gets smoothed until above this threshold. 1.0 results in no smoothing	snr_thresh	2.0
maximum pixel shift allowed for nonrigid, relative to rigid	maxregshiftNR	10
Cell detection		
Run ROI extraction	roidetect	True
Run sparse_mode	sparse_mode	False
Diameter for filtering and extracting	diameter	12.0
Keep ROIs fully connected (set to 0 for dendrites)	connected	True
Maximum number of binned frames for cell detection	nbinned	5000
Maximum number of iterations to do cell detection	max_iterations	20
Adjust the automatically determined threshold by this scalar multiplier	threshold_scaling	1.0 or 0.1

bioRxiv preprint doi: https://doi.org/10.1101/2020.06.05.135905; this version posted June 6, 2020. The copyright holder for this preprint (which was not certified by peer review) is the author/funder. All rights reserved. No reuse allowed without permission.

Cells with more overlap than this get removed during triage, before refinement	max_overlap	0.75
Running mean subtraction with window of size 'high_pass'	high_pass	100
ROI extraction		
Number of pixels to keep between ROI and neuropil donut	inner_neuropil_radius	2
Minimum number of pixels in the neuropil	min_neuropil_pixels	100
Pixels that are overlapping are thrown out (False) or added to both ROIs (True)	allow_overlap	True
Deconvolution		
Deconvolution time constant, seconds	tau	0.7

The same analytical pipeline was applied to both the raw fluorescence traces as well as the deconvolved ("spikes") signal, as extracted by the Suite2p toolbox. Generally, the raw fluorescence signal was preferred over the deconvolved one given that its extraction is more straightforward and relies on less assumptions. However, while the reported effects varied in magnitude depending on which of the two signals was considered, the same results were obtained on both datasets. The effects were entirely consistent. For raw signal analysis of each neuron, previous to any further step, we subtracted 0.7 of the corresponding neuropil fluorescence trace.

The number and height of calcium transients properties were calculated with the scipy function *find_peaks* on the raw calcium traces with the following parameters: height = 200, distance = 10 and prominence = 200. The decay was computed on the 10 best-isolated transients of each neuron, using the *OASIS* toolbox (https://github.com/j-friedrich/OASIS). We used the *deconvolve* function with the following parameters: penalty = 0, optimize_g = 10. Traces with an estimated decay over 2 seconds were considered cases of failed extraction and removed from further analysis.

The choice of the parameter values for transient detection is somewhat arbitrary. Similarly, it is debatable whether and how the calcium traces should best be normalized. Therefore, we tested the robustness of our findings by systematically varying signal extraction choices. We first varied the height and prominence threshold across a wide range of values (50 to 700 arbitrary units). We further computed transients features on normalized ΔF/F calcium traces. To normalize calcium signals, we used the baseline value as extracted by the *deconvolve* function. Also, in this case, we varied the height and prominence threshold across a wide range of values (0.5 to 3 arbitrary units). Finally, we computed two measures of neuronal activity that are independent of calcium transients detection: the average of the trace integral and its standard deviation, with and without normalization. Across all of these scenarios, the reported effects were robustly consistent.

Correlations were computed both as Pearson (numpy function *corrcoeff*) and Spearman (custom written function) coefficient on the z-scored signal. To both sets of coefficients, the

bioRxiv preprint doi: https://doi.org/10.1101/2020.06.05.135905; this version posted June 6, 2020. The copyright holder for this preprint (which was not certified by peer review) is the author/funder. All rights reserved. No reuse allowed without permission.

Fisher correction (the inverse of the hyperbolic tangent function, numpy function *arctanh*) was applied. For power analysis, we first created a population activity vector by summing all the single neuron z-scored signals, and then estimated the power spectral density by applying the Welch method (sampling frequency = 30 Hz, number of points for fast Fourier transformation = 1024, no overlap, window length = 1 s).

Complexity analysis was performed in the Matlab (MathWorks) environment. For complexity analysis, we limited the amount of neurons to the minimum (N_{min}) present in any recording of any condition for each single mouse (median = 265, min = 156, max = 1068). The resulting matrix therefore had the $T_{rec}xN_{min}$ dimensions, where T_{rec} represents the time vector for the recording, with a length of 5 min and a sampling rate of 30 Hz. For recordings that had a number of neurons larger than N_{min} for that mouse, we randomly sampled n = N_{min} neurons and repeated the analysis 5 times. For every extracted parameter, we then considered the median value over the 5 repetitions. For further analysis, the signal was downsampled from the original sampling frequency of 30 Hz to 10 Hz (100 ms bins). The same analytical pipeline was then applied to both the raw fluorescence traces, as well as the deconvolved signal.

tSNE clustering. tSNE clustering was performed similar to (Wenzel et al., 2019). Briefly, in a range between 5 and 45, the perplexity value that minimized the reconstruction error was selected. The number of PCA components used for this step was limited to 30. For the raw fluorescence signal, Euclidian distance was used, whereas for the deconvolved signal we opted for cosine distance, as it is better suited to a sparse signal. We computed the probability distribution of the resulting embedded matrix ($2xT_{rec}$), that was then convolved with a 2D Gaussian window (standard deviation was set to be equal to 1/40 of the total maximum value). To evaluate the number of clusters in the distribution, we then applied a series of standard steps in image analysis: background subtraction with the rolling ball method, smoothing with a median filter, thresholding, watershedding to avoid undersegmentation, and extended minima transformation. Finally, the exterior boundaries of the objects were traced and counted. This gave the number of clusters.

Affinity Propagation Clustering (APC). Affinity Propagation clustering was performed using a Matlab toolbox [https://www.psi.toronto.edu/index.php?q=affinity%20propagation] and similarly to (Wenzel et al., 2019). We first obtained a distance map, which was computed as 1 minus the pairwise cosine distance between observations of the $T_{rec}xN_{min}$ matrix. This distance matrix was then fed to the affinity propagation algorithm with the input preference set equal to the median of the distance matrix.

Principal Component Analysis (PCA) clustering and variance explained. Standard PCA was applied to the $T_{rec}xN_{min}$ matrix. The number of clusters was computed as the number of components that was needed to cumulatively explain 90% of the variance of the input matrix. Further, we computed the loglog decay coefficient of number of components versus variance explained.

Community detection. To detect communities, we used the Louvain algorithm from the Brain Connectivity Toolbox (https://sites.google.com/site/bctnet/), a modularity maximization procedure widely used in studies examining brain networks (Rubinov and Sporns, 2010). This approach aims at subdividing the network into partitions that are more internally dense than would be expected by chance (Sporns and Betzel, 2016). As input to the algorithm, we used Fisher-transformed correlation matrices obtained from calcium imaging time-series. Matrices were not thresholded, and both positive and negative correlations were taken into account to determine optimal modular partitions. The algorithm was evaluated while varying the resolution

bioRxiv preprint doi: https://doi.org/10.1101/2020.06.05.135905; this version posted June 6, 2020. The copyright holder for this preprint (which was not certified by peer review) is the author/funder. All rights reserved. No reuse allowed without permission.

parameter gamma between 0 and 3, in steps of 0.1. For the multiresolution approach and hierarchical consensus clustering, data was analyzed using code available at https://github.com/LJeub/HierarchicalConsensus and according to the procedure described in (Jeub et al., 2018). The number of communities detected by the finest level partition of the consensus hierarchy was used for further analysis. While neurons in the awake condition tended to be spatially closer to each other than for the other conditions (Fig. S10E), this is unlikely to have influenced the results of the analysis, as the difference was minimal and there was no correlation between median distance in a recording and the number of detected communities (Fig. S10F).

Two-Photon Spine Image Processing

In each animal, at least one GFP-expressing CA1 pyramidal neuron was selected and 1-3 dendrites of 20–50 µm length of each of the following types were analyzed: basal dendrites, oblique dendrites emerging from the apical trunk and tuft dendrites. Motion artefacts were corrected with a custom-modified Lucas-Kanade-based alignment algorithm written in Matlab. Spines that laterally emanated from the dendrite were counted by manually scrolling through the z-stacks of subsequent imaging time points of the same dendritic element, by an expert examiner blinded to the experimental condition. Protrusions from the dendrite that reached a threshold of 0.2 µm were scored as dendritic spines regardless of shape. If spine neck positions differed 0.5 µm on the subsequent images, the spine was scored as a new spine. Spines were scored as lost if they fell below the threshold of 0.2 µm. Spine density was calculated as the number of spines per µm. The turnover ratio was calculated for every time point by dividing the sum of gained and lost spines by the number of present spines. The survival fraction of spines was calculated as the percentage of remaining spines compared with the first imaging time point.

Statistical analysis

Statistical analyses were performed using R Statistical Software (Foundation for Statistical Computing, Vienna, Austria) or GraphPad Prism. All R scripts and datasets are available on github https://github.com/mchini/Calcium-Imaging---Anesthesia. Nested data were analyzed with linear mixed-effect models to account for the commonly ignored increased false positive rate inherent in nested design (Aarts et al., 2014). We used “mouse”, “recording”, “neuron” (calcium imaging), and “single unit” (electrophysiology) as random effects, according to the specific experimental design. Parameter estimation was done using the lmer function implemented in the *lme4* R package (Bates et al., 2015). Model selection was performed according to experimental design. Significance and summary tables for lmer model fits were evaluated with the *lmerTest* R package (Kuznetsova et al., 2017), using the Satterthwaite's degrees of freedom method. Post hoc analysis with Tukey multiple comparison correction was carried out using the *emmeans* R package.

REFERENCES

Aarts, E., Verhage, M., Veenvliet, J.V., Dolan, C.V., and van der Sluis, S. (2014). A solution to dependency: using multilevel analysis to accommodate nested data. Nat Neurosci 17, 491-496.

Albrecht, M., Henke, J., Tacke, S., Markert, M., and Guth, B. (2014). Effects of isoflurane, ketamine-xylazine and a combination of medetomidine, midazolam and fentanyl on

bioRxiv preprint doi: https://doi.org/10.1101/2020.06.05.135905; this version posted June 6, 2020. The copyright holder for this preprint (which was not certified by peer review) is the author/funder. All rights reserved. No reuse allowed without permission.

physiological variables continuously measured by telemetry in Wistar rats. BMC Vet Res 10, 198.

Alkire, M.T., Hudetz, A.G., and Tononi, G. (2008). Consciousness and anesthesia. Science 322, 876-880.

Antognini, J.F., and Carstens, E. (2002). In vivo characterization of clinical anaesthesia and its components. Br J Anaesth 89, 156-166.

Attardo, A., Fitzgerald, J.E., and Schnitzer, M.J. (2015). Impermanence of dendritic spines in live adult CA1 hippocampus. Nature 523, 592-596.

Bates, D., Machler, M., Bolker, B.M., and Walker, S.C. (2015). Fitting Linear Mixed-Effects Models Using lme4. J Stat Softw 67, 1-48.

Bittner, K.C., Grienberger, C., Vaidya, S.P., Milstein, A.D., Macklin, J.J., Suh, J., Tonegawa, S., and Magee, J.C. (2015). Conjunctive input processing drives feature selectivity in hippocampal CA1 neurons. Nat Neurosci.

Bonin, R.P., and Orser, B.A. (2008). GABA(A) receptor subtypes underlying general anesthesia. Pharmacol Biochem Behav 90, 105-112.

Briner, A., De Roo, M., Dayer, A., Muller, D., Habre, W., and Vutskits, L. (2010). Volatile anesthetics rapidly increase dendritic spine density in the rat medial prefrontal cortex during synaptogenesis. Anesthesiology 112, 546-556.

Briner, A., Nikonenko, I., De Roo, M., Dayer, A., Muller, D., and Vutskits, L. (2011). Developmental Stage-dependent persistent impact of propofol anesthesia on dendritic spines in the rat medial prefrontal cortex. Anesthesiology 115, 282-293.

Buzsaki, G. (1986). Hippocampal sharp waves: their origin and significance. Brain Res 398, 242-252.

Buzsaki, G., Anastassiou, C.A., and Koch, C. (2012). The origin of extracellular fields and currents--EEG, ECoG, LFP and spikes. Nat Rev Neurosci 13, 407-420.

Canolty, R.T., and Knight, R.T. (2010). The functional role of cross-frequency coupling. Trends in cognitive sciences 14, 506-515.

Chen, G., Chen, K.S., Knox, J., Inglis, J., Bernard, A., Martin, S.J., Justice, A., McConlogue, L., Games, D., Freedman, S.B., and Morris, R.G. (2000). A learning deficit related to age and beta-amyloid plaques in a mouse model of Alzheimer's disease. Nature 408, 975-979.

Chen, T.W., Wardill, T.J., Sun, Y., Pulver, S.R., Renninger, S.L., Baohan, A., Schreiter, E.R., Kerr, R.A., Orger, M.B., Jayaraman, V.*, et al.* (2013). Ultrasensitive fluorescent proteins for imaging neuronal activity. Nature 499, 295-300.

Chini, M., Gretenkord, S., Kostka, J.K., Popplau, J.A., Cornelissen, L., Berde, C.B., Hanganu-Opatz, I.L., and Bitzenhofer, S.H. (2019). Neural Correlates of Anesthesia in Newborn Mice and Humans. Frontiers in neural circuits 13, 38.

Clark, D.L., and Rosner, B.S. (1973). Neurophysiologic effects of general anesthetics. I. The electroencephalogram and sensory evoked responses in man. Anesthesiology 38, 564-582.

Collins, D.R., Pelletier, J.G., and Pare, D. (2001). Slow and fast (gamma) neuronal oscillations in the perirhinal cortex and lateral amygdala. J Neurophysiol 85, 1661-1672.

bioRxiv preprint doi: https://doi.org/10.1101/2020.06.05.135905; this version posted June 6, 2020. The copyright holder for this preprint (which was not certified by peer review) is the author/funder. All rights reserved. No reuse allowed without permission.

Contreras, D., and Steriade, M. (1995). Cellular basis of EEG slow rhythms: a study of dynamic corticothalamic relationships. J Neurosci 15, 604-622.

Cutts, C.S., and Eglen, S.J. (2014). Detecting pairwise correlations in spike trains: an objective comparison of methods and application to the study of retinal waves. J Neurosci 34, 14288-14303.

Dailey, M.E., and Smith, S.J. (1996). The dynamics of dendritic structure in developing hippocampal slices. J Neurosci 16, 2983-2994.

De Roo, M., Klauser, P., Briner, A., Nikonenko, I., Mendez, P., Dayer, A., Kiss, J.Z., Muller, D., and Vutskits, L. (2009). Anesthetics rapidly promote synaptogenesis during a critical period of brain development. PloS one 4, e7043.

De Roo, M., Klauser, P., and Muller, D. (2008). LTP promotes a selective long-term stabilization and clustering of dendritic spines. PLoS Biol 6, e219.

Fleischmann, T., Jirkof, P., Henke, J., Arras, M., and Cesarovic, N. (2016). Injection anaesthesia with fentanyl-midazolam-medetomidine in adult female mice: importance of antagonization and perioperative care. Lab Anim 50, 264-274.

Franks, N.P. (2008). General anaesthesia: from molecular targets to neuronal pathways of sleep and arousal. Nat Rev Neurosci 9, 370-386.

Frey, U., and Morris, R.G. (1997). Synaptic tagging and long-term potentiation. Nature 385, 533-536.

Gao, R., Peterson, E.J., and Voytek, B. (2017). Inferring synaptic excitation/inhibition balance from field potentials. NeuroImage 158, 70-78.

Goltstein, P.M., Montijn, J.S., and Pennartz, C.M. (2015). Effects of isoflurane anesthesia on ensemble patterns of Ca2+ activity in mouse v1: reduced direction selectivity independent of increased correlations in cellular activity. PloS one 10, e0118277.

Greenberg, D.S., Houweling, A.R., and Kerr, J.N. (2008). Population imaging of ongoing neuronal activity in the visual cortex of awake rats. Nat Neurosci 11, 749-751.

Gu, L., Kleiber, S., Schmid, L., Nebeling, F., Chamoun, M., Steffen, J., Wagner, J., and Fuhrmann, M. (2014). Long-term in vivo imaging of dendritic spines in the hippocampus reveals structural plasticity. J Neurosci 34, 13948-13953.

Hardingham, G.E., and Bading, H. (2010). Synaptic versus extrasynaptic NMDA receptor signalling: implications for neurodegenerative disorders. Nat Rev Neurosci.

Harris, K.D., and Mrsic-Flogel, T.D. (2013). Cortical connectivity and sensory coding. Nature 503, 51-58.

Jeub, L.G.S., Sporns, O., and Fortunato, S. (2018). Multiresolution Consensus Clustering in Networks. Scientific reports 8.

Kasai, H., Fukuda, M., Watanabe, S., Hayashi-Takagi, A., and Noguchi, J. (2010). Structural dynamics of dendritic spines in memory and cognition. Trends Neurosci 33, 121-129.

Katz, Y., Menon, V., Nicholson, D.A., Geinisman, Y., Kath, W.L., and Spruston, N. (2009). Synapse distribution suggests a two-stage model of dendritic integration in CA1 pyramidal neurons. Neuron 63, 171-177.

bioRxiv preprint doi: https://doi.org/10.1101/2020.06.05.135905; this version posted June 6, 2020. The copyright holder for this preprint (which was not certified by peer review) is the author/funder. All rights reserved. No reuse allowed without permission.

Klausberger, T., and Somogyi, P. (2008). Neuronal diversity and temporal dynamics: the unity of hippocampal circuit operations. Science 321, 53-57.

Klinzing, J.G., Niethard, N., and Born, J. (2019). Mechanisms of systems memory consolidation during sleep. Nat Neurosci 22, 1598-1610.

Kuznetsova, A., Brockhoff, P.B., and Christensen, R.H.B. (2017). lmerTest Package: Tests in Linear Mixed Effects Models. J Stat Softw 82, 1-26.

Langsjo, J.W., Maksimow, A., Salmi, E., Kaisti, K., Aalto, S., Oikonen, V., Hinkka, S., Aantaa, R., Sipila, H., Viljanen, T.*, et al.* (2005). S-ketamine anesthesia increases cerebral blood flow in excess of the metabolic needs in humans. Anesthesiology 103, 258-268.

Larkum, M. (2012). A cellular mechanism for cortical associations: an organizing principle for the cerebral cortex. Trends Neurosci.

Lee, U., Ku, S., Noh, G., Baek, S., Choi, B., and Mashour, G.A. (2013). Disruption of frontal-parietal communication by ketamine, propofol, and sevoflurane. Anesthesiology 118, 1264-1275.

Lendvai, B., Stern, E.A., Chen, B., and Svoboda, K. (2000). Experience-dependent plasticity of dendritic spines in the developing rat barrel cortex in vivo. Nature 404, 876-881.

Li, N., Lee, B., Liu, R.J., Banasr, M., Dwyer, J.M., Iwata, M., Li, X.Y., Aghajanian, G., and Duman, R.S. (2010). mTOR-dependent synapse formation underlies the rapid antidepressant effects of NMDA antagonists. Science 329, 959-964.

Lin, H., Higgins, P., Loh, H.H., Law, P.Y., and Liao, D. (2009). Bidirectional effects of fentanyl on dendritic spines and AMPA receptors depend upon the internalization of mu opioid receptors. Neuropsychopharmacology 34, 2097-2111.

Mashour, G.A., Orser, B.A., and Avidan, M.S. (2011). Intraoperative awareness: from neurobiology to clinical practice. Anesthesiology 114, 1218-1233.

Mizrahi-Kliger, A.D., Kaplan, A., Israel, Z., and Bergman, H. (2018). Desynchronization of slow oscillations in the basal ganglia during natural sleep. Proc Natl Acad Sci U S A 115, E4274-E4283.

Morellini, F. (2013). Spatial memory tasks in rodents: what do they model? Cell Tissue Res 354, 273-286.

Moscovitch, M., Cabeza, R., Winocur, G., and Nadel, L. (2016). Episodic Memory and Beyond: The Hippocampus and Neocortex in Transformation. Annual review of psychology 67, 105-134.

Nadel, L., and Moscovitch, M. (1997). Memory consolidation, retrograde amnesia and the hippocampal complex. Curr Opin Neurobiol 7, 217-227.

Nagerl, U.V., Eberhorn, N., Cambridge, S.B., and Bonhoeffer, T. (2004). Bidirectional activity-dependent morphological plasticity in hippocampal neurons. Neuron 44, 759-767.

Neves, G., Cooke, S.F., and Bliss, T.V. (2008). Synaptic plasticity, memory and the hippocampus: a neural network approach to causality. Nat Rev Neurosci 9, 65-75.

Newman, M.E., and Girvan, M. (2004). Finding and evaluating community structure in networks. Phys Rev E Stat Nonlin Soft Matter Phys 69, 026113.

bioRxiv preprint doi: https://doi.org/10.1101/2020.06.05.135905; this version posted June 6, 2020. The copyright holder for this preprint (which was not certified by peer review) is the author/funder. All rights reserved. No reuse allowed without permission.

O'Neill, J., Pleydell-Bouverie, B., Dupret, D., and Csicsvari, J. (2010). Play it again: reactivation of waking experience and memory. Trends Neurosci 33, 220-229.

Okun, M., Steinmetz, N., Cossell, L., Iacaruso, M.F., Ko, H., Bartho, P., Moore, T., Hofer, S.B., Mrsic-Flogel, T.D., Carandini, M., and Harris, K.D. (2015). Diverse coupling of neurons to populations in sensory cortex. Nature 521, 511-515.

Onslow, A.C., Bogacz, R., and Jones, M.W. (2011). Quantifying phase-amplitude coupling in neuronal network oscillations. Prog Biophys Mol Biol 105, 49-57.

Pachitariu, M., Stringer, C., Dipoppa, M., Schröder, S., Rossi, L.F., Dalgleish, H., Carandini, M., and Harris, K.D. (2017). Suite2p: beyond 10,000 neurons with standard two-photon microscopy. bioRxiv, 061507.

Pfeiffer, T., Poll, S., Bancelin, S., Angibaud, J., Inavalli, V.K., Keppler, K., Mittag, M., Fuhrmann, M., and Nagerl, U.V. (2018). Chronic 2P-STED imaging reveals high turnover of dendritic spines in the hippocampus in vivo. eLife 7.

Phoumthipphavong, V., Barthas, F., Hassett, S., and Kwan, A.C. (2016). Longitudinal Effects of Ketamine on Dendritic Architecture In Vivo in the Mouse Medial Frontal Cortex. eNeuro 3.

Portera-Cailliau, C., Pan, D.T., and Yuste, R. (2003). Activity-regulated dynamic behavior of early dendritic protrusions: evidence for different types of dendritic filopodia. J Neurosci 23, 7129-7142.

Pryazhnikov, E., Mugantseva, E., Casarotto, P., Kolikova, J., Fred, S.M., Toptunov, D., Afzalov, R., Hotulainen, P., Voikar, V., Terry-Lorenzo, R.*, et al.* (2018). Longitudinal two-photon imaging in somatosensory cortex of behaving mice reveals dendritic spine formation enhancement by subchronic administration of low-dose ketamine. Scientific reports 8, 6464.

Purdon, P.L., Sampson, A., Pavone, K.J., and Brown, E.N. (2015). Clinical Electroencephalography for Anesthesiologists: Part I: Background and Basic Signatures. Anesthesiology 123, 937-960.

Rose, T., Jaepel, J., Hubener, M., and Bonhoeffer, T. (2016). Cell-specific restoration of stimulus preference after monocular deprivation in the visual cortex. Science 352, 1319-1322.

Rossant, C., Kadir, S.N., Goodman, D.F.M., Schulman, J., Hunter, M.L.D., Saleem, A.B., Grosmark, A., Belluscio, M., Denfield, G.H., Ecker, A.S.*, et al.* (2016). Spike sorting for large, dense electrode arrays. Nat Neurosci 19, 634-641.

Rubinov, M., and Sporns, O. (2010). Complex network measures of brain connectivity: Uses and interpretations. NeuroImage 52, 1059-1069.

Rudolph, U., and Antkowiak, B. (2004). Molecular and neuronal substrates for general anaesthetics. Nat Rev Neurosci 5, 709-720.

Sanders, R.D., Tononi, G., Laureys, S., and Sleigh, J.W. (2012). Unresponsiveness not equal unconsciousness. Anesthesiology 116, 946-959.

Sarasso, S., Boly, M., Napolitani, M., Gosseries, O., Charland-Verville, V., Casarotto, S., Rosanova, M., Casali, A.G., Brichant, J.F., Boveroux, P.*, et al.* (2015). Consciousness and Complexity during Unresponsiveness Induced by Propofol, Xenon, and Ketamine. Curr Biol 25, 3099-3105.

bioRxiv preprint doi: https://doi.org/10.1101/2020.06.05.135905; this version posted June 6, 2020. The copyright holder for this preprint (which was not certified by peer review) is the author/funder. All rights reserved. No reuse allowed without permission.

Scheffer-Teixeira, R., Belchior, H., Caixeta, F.V., Souza, B.C., Ribeiro, S., and Tort, A.B. (2012). Theta phase modulates multiple layer-specific oscillations in the CA1 region. Cereb Cortex 22, 2404-2414.

Schmid, L.C., Mittag, M., Poll, S., Steffen, J., Wagner, J., Geis, H.R., Schwarz, I., Schmidt, B., Schwarz, M.K., Remy, S., and Fuhrmann, M. (2016). Dysfunction of Somatostatin-Positive Interneurons Associated with Memory Deficits in an Alzheimer's Disease Model. Neuron 92, 114-125.

Schomburg, E.W., Fernandez-Ruiz, A., Mizuseki, K., Berenyi, A., Anastassiou, C.A., Koch, C., and Buzsaki, G. (2014). Theta phase segregation of input-specific gamma patterns in entorhinal-hippocampal networks. Neuron 84, 470-485.

Segal, M. (2005). Dendritic spines and long-term plasticity. Nat Rev Neurosci 6, 277-284.

Sheintuch, L., Rubin, A., Brande-Eilat, N., Geva, N., Sadeh, N., Pinchasof, O., and Ziv, Y. (2017). Tracking the Same Neurons across Multiple Days in Ca(2+) Imaging Data. Cell reports 21, 1102-1115.

Soltesz, I., and Deschenes, M. (1993). Low- and high-frequency membrane potential oscillations during theta activity in CA1 and CA3 pyramidal neurons of the rat hippocampus under ketamine-xylazine anesthesia. J Neurophysiol 70, 97-116.

Sporns, O., and Betzel, R.F. (2016). Modular Brain Networks. Annual review of psychology 67, 613-640.

Steriade, M., Nunez, A., and Amzica, F. (1993). A novel slow (< 1 Hz) oscillation of neocortical neurons in vivo: depolarizing and hyperpolarizing components. J Neurosci 13, 3252-3265.

Sur, C., Fresu, L., Howell, O., McKernan, R.M., and Atack, J.R. (1999). Autoradiographic localization of alpha5 subunit-containing GABAA receptors in rat brain. Brain Res 822, 265-270.

Thevenaz, P., Ruttimann, U.E., and Unser, M. (1998). A pyramid approach to subpixel registration based on intensity. IEEE Trans Image Process 7, 27-41.

Urban, B.W., and Bleckwenn, M. (2002). Concepts and correlations relevant to general anaesthesia. Br J Anaesth 89, 3-16.

Vinck, M., Battaglia, F.P., Womelsdorf, T., and Pennartz, C. (2012). Improved measures of phase-coupling between spikes and the Local Field Potential. J Comput Neurosci 33, 53-75.

Vinck, M., van Wingerden, M., Womelsdorf, T., Fries, P., and Pennartz, C.M. (2010). The pairwise phase consistency: a bias-free measure of rhythmic neuronal synchronization. NeuroImage 51, 112-122.

Vutskits, L., and Xie, Z. (2016). Lasting impact of general anaesthesia on the brain: mechanisms and relevance. Nat Rev Neurosci 17, 705-717.

Wenzel, M., Han, S., Smith, E.H., Hoel, E., Greger, B., House, P.A., and Yuste, R. (2019). Reduced Repertoire of Cortical Microstates and Neuronal Ensembles in Medically Induced Loss of Consciousness. Cell Syst 8, 467-474 e464.

West, A.E., Griffith, E.C., and Greenberg, M.E. (2002). Regulation of transcription factors by neuronal activity. Nat Rev Neurosci 3, 921-931.

bioRxiv preprint doi: https://doi.org/10.1101/2020.06.05.135905; this version posted June 6, 2020. The copyright holder for this preprint (which was not certified by peer review) is the author/funder. All rights reserved. No reuse allowed without permission.

Whitlock, J.R., Heynen, A.J., Shuler, M.G., and Bear, M.F. (2006). Learning induces long-term potentiation in the hippocampus. Science 313, 1093-1097.

Wiegert, J.S., and Bading, H. (2011). Activity-dependent calcium signaling and ERK-MAP kinases in neurons: a link to structural plasticity of the nucleus and gene transcription regulation. Cell calcium 49, 296-305.

Wiegert, J.S., and Oertner, T.G. (2013). Long-term depression triggers the selective elimination of weakly integrated synapses. Proc Natl Acad Sci U S A 110, E4510-4519.

Wiegert, J.S., Pulin, M., Gee, C.E., and Oertner, T.G. (2018). The fate of hippocampal synapses depends on the sequence of plasticity-inducing events. eLife 7.

Yamakage, M., Hirshman, C.A., and Croxton, T.L. (1995). Inhibitory effects of thiopental, ketamine, and propofol on voltage-dependent Ca2+ channels in porcine tracheal smooth muscle cells. Anesthesiology 83, 1274-1282.

Yang, G., Chang, P.C., Bekker, A., Blanck, T.J., and Gan, W.B. (2011). Transient effects of anesthetics on dendritic spines and filopodia in the living mouse cortex. Anesthesiology 115, 718-726.

Yang, G., Pan, F., and Gan, W.B. (2009). Stably maintained dendritic spines are associated with lifelong memories. Nature 462, 920-924.

Yang, Y., Cui, Y., Sang, K., Dong, Y., Ni, Z., Ma, S., and Hu, H. (2018). Ketamine blocks bursting in the lateral habenula to rapidly relieve depression. Nature 554, 317-322.

Zurek, A.A., Bridgwater, E.M., and Orser, B.A. (2012). Inhibition of alpha5 gamma-Aminobutyric acid type A receptors restores recognition memory after general anesthesia. Anesth Analg 114, 845-855.

Zurek, A.A., Yu, J., Wang, D.S., Haffey, S.C., Bridgwater, E.M., Penna, A., Lecker, I., Lei, G., Chang, T., Salter, E.W., and Orser, B.A. (2014). Sustained increase in alpha5GABAA receptor function impairs memory after anesthesia. J Clin Invest 124, 5437-5441.